

# Systemic Risk in Market Microstructure of Crude Oil and Gasoline Futures Prices: A Hawkes Flocking Model Approach

Hyun Jin Jang<sup>1</sup> , Kiseop Lee<sup>2</sup> , Kyungsub Lee<sup>3</sup>

---

## Abstract

We propose a novel class of Hawkes-based model that assesses two types of systemic risk in high-frequency price processes: the endogenous systemic risk within a single process and the interactive systemic risk between a couple of processes. We examine the existence of systemic risk at a microscopic level via an empirical analysis of the futures markets of the West Texas Intermediate (WTI) crude oil and gasoline and perform a comparative analysis with the conditional value-at-risk as a benchmark measure of the proposed model. Throughout the analysis, we uncover remarkable empirical findings in terms of the high-frequency structure of the two markets: for the past decade, the level of endogenous systemic risk in the WTI market was significantly higher than that in the gasoline market. Moreover, the level at which the gasoline price affects the WTI price was constantly higher than in the opposite case. Although the two prices interact with each other at the transaction-unit level, the degree of relative influences on the two markets, that is, from the WTI to the gasoline and vice versa, was very asymmetric, but that difference has reduced gradually over time.

*Key words:* Systemic risk, Hawkes process, flocking, WTI crude oil futures, gasoline futures, calibration, branch ratio, CoVaR

*JEL:* G13, C63, C22

---

## 1. Introduction

Over the past two decades, the level of systemic risk has increased in financial markets due to the growth of securitization, hedge fund markets, and increase in intraday trading. Recently, the emergence of innovative technologies has accelerated the paradigm shift of

---

<sup>1</sup>School of Management Engineering, School of Business Administration, Ulsan National Institute of Science and Technology (UNIST), Republic of Korea, Email: janghj@unist.ac.kr

<sup>2</sup>Department of Statistics, Purdue University, Email: kiseop@purdue.edu

<sup>3</sup>Department of Statistics, Yeungnam University, Gyeongsan, Republic of Korea, Corresponding author, Email: ksublee@yu.ac.kr

trading activities in financial markets. Traditional trading platforms such as phone conversations or a click on a screen by humans has moved to automated trading by computers based on the ultra-low latency electronic system. The increased trading speed enables execution of orders within microseconds by the use of sophisticated algorithms; this is called high-frequency trading. According to a report of the Commodity Futures Trading Commission (CFTC)<sup>4</sup>, the volume of high-frequency trading in futures markets has grown remarkably over the past decade. This accounts for 80% of foreign exchange futures, 67% of interest rate futures, 62% of equity futures, and 47% of metals and energy futures trading volume. Such an environmental change in trading potentially allows large price movements within a short period of time as well as the rapid risk propagation to different assets, as mentioned in [Miller and Shorter \(2016\)](#).

In this context of high-frequency finance, we develop a novel Hawkes process-based model to examine the level of systemic risk that exists within and between price dynamics at the microscopic level. The proposed model allows capturing contagious and clustered phenomena that can be investigated in the excessive volatile and correlated markets. Studies related to systemic risk in high-frequency trading are discussed under various aspects. [Filimonov and Sornette \(2012\)](#) conduct event studies to investigate the changes in the systemic risk before and after the announcements of two extreme events: downgrading of Greece/Portugal and the “flash crash” event for the E-mini S&P500 futures in 2010. [Hardiman et al. \(2013\)](#) perform a similar analysis with [Filimonov and Sornette \(2012\)](#) by taking power-law kernels. [Chavez-Demoulin and McGill \(2012\)](#) compute intraday value-at-risk (VaR) for stocks in New York Stock Exchange (NYSE) using a peak-over-threshold model, and [Jain et al. \(2016\)](#) assess the extent to which a high-frequency system increases systemic risk in the Tokyo Stock Exchange. [Bormetti et al. \(2015\)](#) use a multivariate Hawkes process with a common factor that controls a large number of jumps in the transaction movement. [Calcagnile et al. \(2018\)](#) compute the number of co-jumps occurring in Russell 3000 index stocks to measure the frequency of the collective instability at high-frequency.

On the other hand, there is little discussion on the increased level of systemic risk in energy markets associated with high-frequency trading. However, energy futures markets are no longer exceptional on this matter. As noted in the beginning, almost the half of the trading volume in the energy markets is raised from high-frequency trading. Moreover, when the Dow Jones Industrial Average had a flash crash event on August 24, 2015,

---

<sup>4</sup>CFTC, “Remarks of Chairman Timothy Massad before the Conference on the Evolving Structure of the US Treasury Market,” October 21, 2015, at <http://www.cftc.gov/PressRoom/SpeechesTestimony/opamassad-30>.

it plunged roughly 1,100 points in the first five minutes of trading. Hence, the CFTC examined the frequency of flash events in the top-five most active futures contracts for 2015, that is, corn, gold, West Texas Intermediate (WTI) crude oil, E-mini S&P 500 futures, and Euro FX. Among them, surprisingly, more than 35 similar intraday flash have occurred just for WTI crude oil futures. This result implies that WTI crude oil futures utilized actively as instruments of algorithmic trading strategies.

Moreover, gasoline futures contracts are being traded most actively in the New York Mercantile Exchange (NYMEX) in the energy sector, following the WTI crude oil futures. Futures prices of the WTI crude oil and the gasoline have maintained a strong dependence for a long time. From the macroeconomic perspective, the main causes of the price difference between crude oil and gasoline are refining costs and supply/demand balance of each product. In addition, such comovement has been studied in terms of market integration or flocking behavior in an econometric field (see, e.g., Granger, 1981; Chiu et al., 2015; Ha et al., 2015; Fang et al., 2017). When the two markets are integrated or have flocking behavior, the associated prices are closely correlated. Furthermore, one price could lead the other, while the reverse also occurs from time to time, or all prices in a system could follow the same behavior.

In this study, we attempt to discover empirical evidence of the systemic risk level in the dynamics of the two futures prices of WTI crude oil and gasoline observed at the intraday transaction level over the past decade. We consider two kinds of definitions for systemic risk in the market microstructure with the instability perspective. The first view is the degree of instability that exists within a price process. It is regarded as the term *endogeneity*, which is introduced in the earlier literature (e.g., Danielsson et al., 2012; Filimonov and Sornette, 2012; Hardiman et al., 2013<sup>5</sup>). By estimating this level, we examine whether the trend of price decline leads to additional price decreases (or price rebounds). The second view is the degree of instability that exists between price processes caused by *interaction* between two different markets. In that point of view, we investigate how the change in one price affects to the change in the other price, and vice versa. In addition, we observe how micro-movements of prices in the two markets are related each other when the price difference widens or narrows.

Based on the notions of systemic risk in a high-frequency market, we propose a *Hawkes flocking model* that enables us to quantify the level of systemic risk embedded in price structures at a microscopic level. This model addresses how to measure the extent of both

---

<sup>5</sup>In Filimonov and Sornette (2012) and Hardiman et al. (2013), this is referred to “reflexivity” instead of endogeneity

endogeneity and interactivity. By manipulating intensity processes that depend on the relative level of a couple of prices, the proposed model describes the self- and mutually-exciting features as well as the flocking behavior mechanism. Moreover, as direct indicators of systemic risk, we formulate branch ratios, which are generally used in a Hawkes-based model to gauge how many additional jumps occur in the intensity process due to one exogenous event for checking the stability of the process. For the empirical analysis, we choose the nearest dated futures prices of WTI crude oil and gasoline that are collected at a transaction level in the time period of January 2007 to December 2016. During this period, prices plunged three times in both markets.

We also compute the level of systemic risk by employing an existing methodology, that is, a conditional value-at-risk (CoVaR) approach, as a complementary measure of the proposed model. The concept of CoVaR is that the maximum loss can happen in an entity within a confidence level due to the effect of large loss from the other entity. This was firstly proposed by [Adrian and Brunnermeier \(2016\)](#) and generalized by [Girardi and Ergun \(2013\)](#). In this study, we adopt the CoVaR defined by [Girardi and Ergun \(2013\)](#) and use a copula method to implement the CoVaR introduced by [Reboredo and Ugolini \(2015\)](#). Then, we simulate the results from the CoVaR method and from the Hawkes flocking model and compare the evolution of systemic risk in the high-frequency markets of WTI crude oil and gasoline, which interplay actively.

The main contribution of this study is twofold. First, we develop a novel class of Hawkes-based model that assesses two types of systemic risk in high-frequency price processes: the endogenous systemic risk in a single process and interactive systemic risk in a couple of processes. Second, we examine the existence of the systemic risk at a microscopic level via the futures markets of WTI crude oil and gasoline that are most liquid in the US energy sector. Through the empirical test based on the proposed model, we obtained the following results. The overall systemic risk level that exists in the two futures markets was the highest just before the onset of the global credit crisis. For the past decade, the level of endogeneity in the WTI market was significantly higher than that in the gasoline market. In particular, the level at which gasoline price affects WTI price was steadily higher than in the opposite case. Although the two markets have been interactive, their relative influences, that is, from WTI to gasoline and vice versa, were very asymmetric, but the degree of the difference has been gradually reducing over the study period.

This paper is organized as follows. In [Section 2](#), we introduce the Hawkes flocking model and derive branch ratios to check the stability condition of the process. [Section 3](#) presents the intraday transaction data for the two futures prices of WTI crude oil and gasoline from 2007 to 2016 along with estimate results under the proposed model using

the maximum likelihood (ML) method. Section 4 presents a comparative analysis between the branch ratios of the proposed model and the CoVaR measure. Section 5 concludes the paper, and technical proofs and additional figures/tables are presented in the Appendix.

## 2. A Hawkes Flocking Model

In this section, we develop a Hawkes flocking model. The proposed model can be categorized to generalized Hawkes processes, which is introduced in the serial papers (Hawkes, 1971a; Hawkes, 1971b; Hawkes and Oakes, 1974). As the Hawkes process is based on a class of multivariate counting processes, this model can account for the interaction of various types of Poisson-like events through its intensity process.

Because of their great flexibility and versatility, Hawkes-based models are very popular for modeling high-frequency finance. A Hawkes model assumes that market price change is essentially driven by two components: the balance of the supply/demand and an endogenous feedback that incorporates market participants with fundamental price change. As a pioneering work, Bowsher (2007) introduce a bivariate Hawkes processes to model the joint dynamics of trades and mid-price changes in NYSE stocks. After that, many studies related to high-frequency finance have employed Hawkes processes (Bacry et al., 2012; Bacry et al., 2013; Da Fonseca and Zaatour, 2014; Bacry et al., 2015; Lee and Seo, 2017).

As noted in the introduction, the model we propose captures the interaction between two highly correlated processes observed at the level of transaction data. Consider the bivariate price processes that are defined by the differences between the two counting processes:

$$\begin{aligned} C_1(t) &= \delta_1(N_1^u(t) - N_1^d(t)) \\ C_2(t) &= \delta_2(N_2^u(t) - N_2^d(t)) \end{aligned}$$

where processes  $N_i^u(t)$  and  $N_i^d(t)$  count the number of events for upward and downward movement in price  $C_i(t)$  up to time  $t$ , respectively, and  $\delta_i$  are tick sizes.

We present a system of the counting process  $\mathbf{N}$  and its intensity process  $\boldsymbol{\lambda}$  by employing the following matrix form

$$\mathbf{N}_t = \begin{bmatrix} N_1^u(t) \\ N_1^d(t) \\ N_2^u(t) \\ N_2^d(t) \end{bmatrix}, \quad \boldsymbol{\lambda}_t = \begin{bmatrix} \lambda_1^u(t) \\ \lambda_1^d(t) \\ \lambda_2^u(t) \\ \lambda_2^d(t) \end{bmatrix}$$

where intensity process  $\lambda$  represents the expected number of arrivals of counting events over an infinitesimal time interval  $dt$  divided by  $dt$ . Let the intensity process be

$$\lambda_t = \boldsymbol{\mu} + \int_{-\infty}^t \mathbf{h}(t-u) d\mathbf{N}_u \quad (1)$$

where  $\boldsymbol{\mu} = [\mu_1, \mu_1, \mu_2, \mu_2]^\top$  is a constant vector, and  $\mathbf{h}$  is a four-by-four matrix. Here, the vector  $\boldsymbol{\mu}$  is called base intensity that accounts for the average frequency of exogenous events coming into this system, which is independent of the other asset's movement as well as its past movement. Parameters  $\mu_1$  and  $\mu_2$  are interpreted as the pressure of orders for buying or selling at price  $C_1$  and  $C_2$ , respectively. The matrix  $\mathbf{h}$  is called a feedback kernel of the Hawkes process that decides the weight to be attributed to events  $d\mathbf{N}$  occurring at lag  $u$  in the past.

We set the feedback kernel by

$$\mathbf{h}(t-u) = \boldsymbol{\Phi}(t-u) + \mathbf{k}(t) \circ \boldsymbol{\Psi}(t-u) \quad (2)$$

where  $\boldsymbol{\Phi}$ ,  $\mathbf{k}$ , and  $\boldsymbol{\Psi}$  are four-by-four matrices, and “ $\circ$ ” denotes the element-wise multiplication of matrices. Kernel  $\mathbf{h}$  consists of two components:

- (i) The matrix  $\boldsymbol{\Phi}$  controls the self- and mutually-exciting patterns between the two prices, which are defined as

$$\boldsymbol{\Phi}(t) = \begin{bmatrix} \alpha_{1s}e^{-\beta_1 t} & \alpha_{1c}e^{-\beta_1 t} & 0 & 0 \\ \alpha_{1c}e^{-\beta_1 t} & \alpha_{1s}e^{-\beta_1 t} & 0 & 0 \\ 0 & 0 & \alpha_{2s}e^{-\beta_2 t} & \alpha_{2c}e^{-\beta_2 t} \\ 0 & 0 & \alpha_{2c}e^{-\beta_2 t} & \alpha_{2s}e^{-\beta_2 t} \end{bmatrix} \quad (3)$$

where non-negative constants  $\alpha_{is}$  and  $\alpha_{ic}$  denote the self- and mutually-exciting terms, respectively, and  $\beta_i$  governs the speed of decay to the base intensity level of the  $i$ -th price process.

- (ii) The matrix  $\mathbf{k} \circ \boldsymbol{\Psi}$  controls the flocking phenomenon according to which two price movements interact, and where matrix  $\mathbf{k}$  is defined by an indicator function matrix such as

$$\mathbf{k}(t) = \begin{bmatrix} \mathbb{1}_{\{C_1(t) < C_2(t)\}} & \mathbb{1}_{\{C_1(t) < C_2(t)\}} & \mathbb{1}_{\{C_1(t) < C_2(t)\}} & \mathbb{1}_{\{C_1(t) < C_2(t)\}} \\ \mathbb{1}_{\{C_1(t) > C_2(t)\}} & \mathbb{1}_{\{C_1(t) > C_2(t)\}} & \mathbb{1}_{\{C_1(t) > C_2(t)\}} & \mathbb{1}_{\{C_1(t) > C_2(t)\}} \\ \mathbb{1}_{\{C_2(t) < C_1(t)\}} & \mathbb{1}_{\{C_2(t) < C_1(t)\}} & \mathbb{1}_{\{C_2(t) < C_1(t)\}} & \mathbb{1}_{\{C_2(t) < C_1(t)\}} \\ \mathbb{1}_{\{C_2(t) > C_1(t)\}} & \mathbb{1}_{\{C_2(t) > C_1(t)\}} & \mathbb{1}_{\{C_2(t) > C_1(t)\}} & \mathbb{1}_{\{C_2(t) > C_1(t)\}} \end{bmatrix}, \quad (4)$$

and the matrix  $\Psi(t)$  is defined by

$$\Psi(t) = \begin{bmatrix} 0 & 0 & \alpha_{1w}e^{-\beta_1 t} & \alpha_{1n}e^{-\beta_1 t} \\ 0 & 0 & \alpha_{1n}e^{-\beta_1 t} & \alpha_{1w}e^{-\beta_1 t} \\ \alpha_{2w}e^{-\beta_2 t} & \alpha_{2n}e^{-\beta_2 t} & 0 & 0 \\ \alpha_{2n}e^{-\beta_2 t} & \alpha_{2w}e^{-\beta_2 t} & 0 & 0 \end{bmatrix} \quad (5)$$

where non-negative constants  $\alpha_{iw}$  and  $\alpha_{in}$  denote the flocking exciting terms.

In part (i), the exponential decaying setup in the bivariate Hawkes process with symmetric  $\alpha$ 's shows a prototypical model for high-frequency finance. In part (ii),  $\mathbf{k}$  deals with the flocking phenomenon while considering an additional term under which intensity  $\lambda_1^u$  increases only when  $C_1$  is less than  $C_2$  and  $\lambda_1^d$  increases only when  $C_1$  is larger than  $C_2$ .  $\Psi$  captures the degree of a flocking phenomenon. The parameter  $\alpha_{iw}$  or  $\alpha_{in}$  is triggered depending on whether the difference between the two prices is narrowed ( $n$ ) or widened ( $w$ ).

Figure 1 shows a descriptive idea on the intensity movements in a Hawkes flocking model. In this figure, the paths represent the dynamics of two prices and the associated four intensities<sup>6</sup>. The black straight line is for price movement  $C_1$ . The black curved line and curved dashed line represent the intensities for upward and downward movement, respectively. Accordingly, the red lines are for price  $C_2$  and its intensities. Assume  $C_1 > C_2$ .

- A widening upward jump of  $C_1$  occurs, and there are three simultaneous jumps in intensities,  $\lambda_1^u$ ,  $\lambda_1^d$  and  $\lambda_2^u$ . Jumps in  $\lambda_1^u$  and  $\lambda_1^d$  are due to self-and mutually-exciting features in the individual Hawkes model and the jump sizes are  $\alpha_{1s}$  and  $\alpha_{1c}$ , respectively. Jump in  $\lambda_2^u$  is due to the flocking feature to accelerate the upward movement of  $C_2$  resulting from the jump in  $C_1$  and the jump size is  $\alpha_{2w}$ .
- When a narrowing upward movement of  $C_2$  occurs, there are simultaneous jumps in intensities,  $\lambda_2^u$ ,  $\lambda_2^d$  and  $\lambda_1^d$ , similar to before. Jumps in  $\lambda_2^u$  and  $\lambda_2^d$  are due to self-and mutually-exciting features, and jump in  $\lambda_1^d$  is due to the flocking mechanism with a narrowing event. Note that jump sizes of  $\lambda_1^d$  and  $\alpha_{1n}$ , are intentionally expressed as quite small in the figure, since the jumps in intensities due to the narrowing event are close to zero in the empirical analysis.

---

<sup>6</sup>This is for an illustrative purpose and the actual values of prices and intensities may be different from the figure.

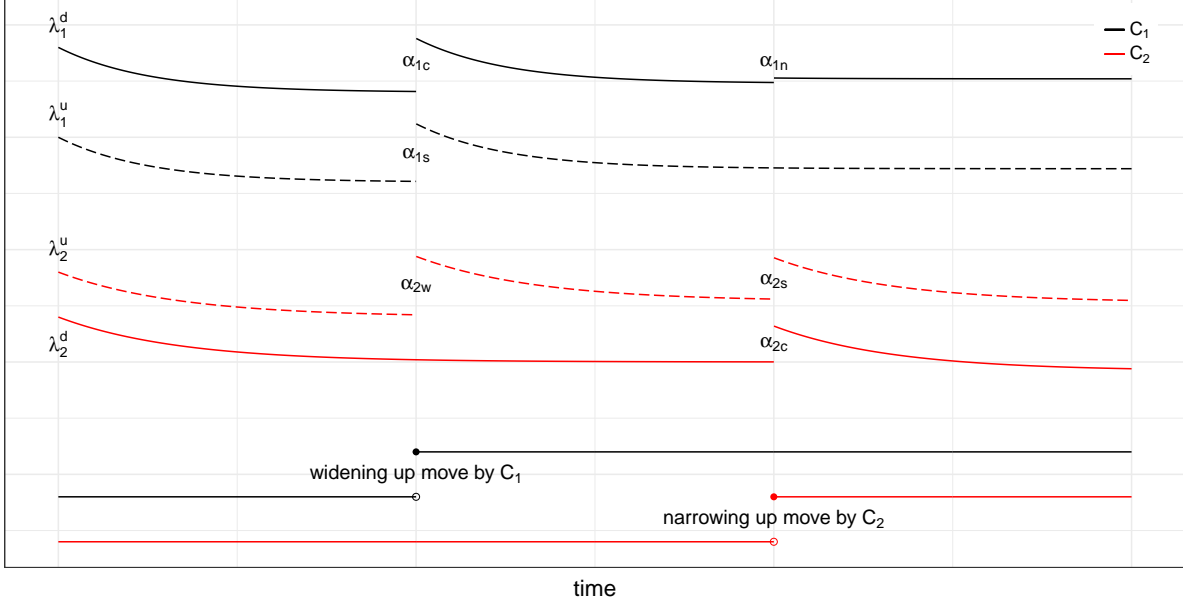


Figure 1: Illustration of the idea on the Hawkes flocking model

**Remark 1** (The role of  $\mathbf{k}$ ). We simply put  $\Phi_{ij} = 0$  and  $\Psi_{ij} = 1$  for all  $i, j$ . Then

$$\lambda_1^u(t) = \mu_1 + \int_{-\infty}^t \mathbb{1}_{\{C_1(u) < C_2(u)\}} d(N_1^u + N_1^d + N_2^u + N_2^d)(u)$$

and this implies that the intensity of the up movement of  $C_1$  changes (typically increases) when  $C_1(t)$  is less than  $C_2(t)$ .

When  $C_1(t) < C_2(t)$ , the intensity of the up movement of  $C_1$  increases, and  $C_1$  and  $C_2$  tend to be close to each other, indicating a flocking phenomenon. With similar arguments, when  $C_1(t) < C_2(t)$ , the up movement of  $C_1$  and down movement of  $C_2$  tend to increase and when  $C_1(t) > C_2(t)$ , the down movement of  $C_1$  and up movement of  $C_2$  tend to increase.

**Remark 2** (Comparison between  $\Phi$  and  $\Psi$ ). Matrices  $\Phi$  and  $\Psi$  have zero components in positions that do not overlap each other. This ensures each role of the matrix is separated:  $\Phi$  only affects the movements in the individual price process, and  $\Psi$  only controls the effect of the new information from another prices process. Therefore, the test of the significance of  $\Psi$  verifies the existence of interactions between the two prices, especially through the sign of  $C_1 - C_2$ .

Through combination with  $\mathbf{k}$ ,  $\alpha_{in}$ , and  $\alpha_{iw}$  respectively represent the effects of the narrowing and widening events of price difference on intensities. To see this, we simply

put  $\Phi_{ij} = 0$ , and then

$$\lambda_1^u(t) = \mu_1 + \int_{-\infty}^t \mathbb{1}_{\{C_1(u) < C_2(u)\}} e^{-\beta_1(t-u)} \left( \alpha_{1w} dN_2^u(u) + \alpha_{1n} dN_2^d(u) \right).$$

When  $C_1(u) < C_2(u)$ , the increase of  $N_2^u(u)$  is the price difference widening event, and the occurrence of  $N_2^d$  is the price difference narrowing event.

From the setup for the components in the kernel matrix  $\mathbf{h}$ , the proposed model can be expressed with a differential form using a Markov property. Let the decay parameter for  $C_1$  and  $C_2$  be fixed as  $\beta_1$  and  $\beta_2$ , respectively. Then, the intensity process satisfies the system of stochastic differential equations such as

$$d\lambda_t = \beta \circ (\mu - \lambda_t) dt + \alpha dN_t$$

where  $\alpha$  and  $\beta$  are given as

$$\alpha = \begin{bmatrix} \alpha_{1s} & \alpha_{1c} & \mathbb{1}_{\{C_1(t) < C_2(t)\}} \alpha_{1w} & \mathbb{1}_{\{C_1(t) < C_2(t)\}} \alpha_{1n} \\ \alpha_{1c} & \alpha_{1s} & \mathbb{1}_{\{C_1(t) > C_2(t)\}} \alpha_{1n} & \mathbb{1}_{\{C_1(t) > C_2(t)\}} \alpha_{1w} \\ \mathbb{1}_{\{C_2(t) < C_1(t)\}} \alpha_{2w} & \mathbb{1}_{\{C_2(t) < C_1(t)\}} \alpha_{2n} & \alpha_{2s} & \alpha_{2c} \\ \mathbb{1}_{\{C_2(t) > C_1(t)\}} \alpha_{2n} & \mathbb{1}_{\{C_2(t) > C_1(t)\}} \alpha_{2w} & \alpha_{2c} & \alpha_{2s} \end{bmatrix}, \quad \beta = \begin{bmatrix} \beta_1 \\ \beta_1 \\ \beta_2 \\ \beta_2 \end{bmatrix}.$$

We understand this model as follows. Market orders (buy or sell) arrive with intensity  $\mu$ , and the arrival intensity jumps by the amount of  $\alpha$  instantly when an arrival event occurs, and then it decays to the base intensity level  $\mu$  with the speed of  $\beta$ .

In Hawkes-based models, the spectral radius defined by the largest absolute value of the eigenvalues of matrix  $\int_0^\infty \mathbf{h}(\tau) d\tau$ , a so-called branch matrix, is used to check the stability condition of the process. According to the ancestor-offspring argument, the immigrant ancestor arrives at the system from the outside at a Poisson intensity rate  $\mu$ , and this ancestor generates offspring with the time-varying rate defined by  $\Phi$  and  $\Psi$ . This generation is continued by both external immigrants and internal offspring. If the spectral radius is strictly less than one, then each ancestor, whether an immigrant or not, generates less than one offspring event on average and hence the process is stable. Otherwise, it diverges to an infinite value within a finite time.

Using an analysis similar to the one for the stability condition in the Hawkes flocking model, we derive a branch matrix of the proposed model, such as

$$\mathbf{M} = \left[ \int_0^\infty |\Phi_{ij}(t) + \mathbb{E}[k_{ij}(t)] \Psi_{ij}(t)| dt \right]_{i,j},$$

for  $i, j = 1, \dots, 4$ . This indicates the average number of offspring events caused by one exogenous event coming in with rate  $\mu$ . To make the matrix  $\mathbf{M}$  symmetric, we suppose

the unconditional expectation  $\mathbb{E}[k_{ij}(t)] = \mathbb{P}\{C_1(t) > C_2(t)\} = \mathbb{P}\{C_1(t) < C_2(t)\} = p \leq 0.5$ <sup>7</sup>. Therefore, we have

$$\mathbf{M} = \begin{bmatrix} \frac{\alpha_{1s}}{\beta_1} & \frac{\alpha_{1c}}{\beta_1} & p\frac{\alpha_{1w}}{\beta_1} & p\frac{\alpha_{1n}}{\beta_1} \\ \frac{\alpha_{1c}}{\beta_1} & \frac{\alpha_{1s}}{\beta_1} & p\frac{\alpha_{1n}}{\beta_1} & p\frac{\alpha_{1w}}{\beta_1} \\ p\frac{\alpha_{2w}}{\beta_2} & p\frac{\alpha_{2n}}{\beta_2} & \frac{\alpha_{2s}}{\beta_2} & \frac{\alpha_{2c}}{\beta_2} \\ p\frac{\alpha_{2n}}{\beta_2} & p\frac{\alpha_{2w}}{\beta_2} & \frac{\alpha_{2c}}{\beta_2} & \frac{\alpha_{2s}}{\beta_2} \end{bmatrix}, \quad (6)$$

and the spectral radius of  $\mathbf{M}$  is obtained by

$$\rho_{\mathbf{M}} = \frac{1}{2}(a + \sqrt{a^2 + 4(b - c)}) \quad (7)$$

where  $a$ ,  $b$ , and  $c$  are given by

$$\begin{aligned} a &= \frac{\alpha_{1s} + \alpha_{1c}}{\beta_1} + \frac{\alpha_{2s} + \alpha_{2c}}{\beta_2}, \\ b &= p^2 \frac{\alpha_{1n}\alpha_{2n} + \alpha_{1n}\alpha_{2w} + \alpha_{1w}\alpha_{2n} + \alpha_{1w}\alpha_{2w}}{\beta_1\beta_2}, \\ c &= \frac{\alpha_{1s}\alpha_{2s} + \alpha_{1s}\alpha_{2c} + \alpha_{1c}\alpha_{2s} + \alpha_{1c}\alpha_{2c}}{\beta_1\beta_2}. \end{aligned}$$

In addition, let  $\Lambda$  be the unconditional expectation of the intensity  $\Lambda = \mathbb{E}[\lambda_t]$ . By considering the expectation of the both sides of (1), we have

$$\begin{aligned} \Lambda &= \boldsymbol{\mu} + \mathbb{E} \left[ \int_{-\infty}^t \Phi(t - u) + \mathbf{k}(u) \circ \Psi(t - u) d\mathbf{N}_u \right] \\ &= \boldsymbol{\mu} + \int_{-\infty}^t \mathbb{E}[(\Phi(t - u) + \mathbf{k}(u) \circ \Psi(t - u))\lambda_u] du \\ &= \boldsymbol{\mu} + \int_{-\infty}^t (\Phi(t - u) + p\Psi(t - u)) \Lambda du \\ &= \boldsymbol{\mu} + \mathbf{M}\Lambda. \end{aligned}$$

Under the stationarity condition, the mean rate of the matrix is represented as

$$\Lambda = (\mathbf{I} - \mathbf{M})^{-1} \boldsymbol{\mu}.$$

To summarize, the Hawkes flocking model has the following characteristics. Each price process has a self- and mutually-exciting term that is affected by its own changes for tick price dynamics. In addition, there is a flocking phenomenon between prices depending on the narrowing or widening events. Moreover, there exists direct mapping between process  $\mathbf{N}_t$  and branch matrix  $\mathbf{M}$ , in which the exogenous main events occur with intensity  $\boldsymbol{\mu}$  and may give rise to additional endogenous following events with mean rate  $\mathbf{M}$ .

---

<sup>7</sup>In our empirical analysis later,  $p$  is quite close to 0.5.

**Remark 3** (Extension of a multi-dimensional Hawkes flocking model). Consider  $m$ -dimensional price processes such that

$$C_1(t) = N_1^u(t) - N_1^d(t), \quad \dots, \quad C_m(t) = N_m^u(t) - N_m^d(t), \quad (8)$$

where processes  $N_i^u(t)$  and  $N_i^d(t)$  have intensity processes  $\lambda_i^u(t)$  and  $\lambda_i^d(t)$ , respectively, for each  $i = 1, \dots, m$ . For a system of  $2m$ -dimensional counting process  $\mathbf{N}$  and its intensity process  $\boldsymbol{\lambda}$

$$\mathbf{N}_t = \begin{bmatrix} N_1^u(t) \\ N_1^d(t) \\ \vdots \\ N_m^u(t) \\ N_m^d(t) \end{bmatrix}, \quad \boldsymbol{\lambda}_t = \begin{bmatrix} \lambda_1^u(t) \\ \lambda_1^d(t) \\ \vdots \\ \lambda_m^u(t) \\ \lambda_m^d(t) \end{bmatrix}$$

we can extend the intensity process in (1) with the feedback kernel in (2) to the multi-dimensional version as follows.

(i) The matrix  $\Phi$  in (3) is given as the  $2m$ -by- $2m$  sized form,

$$\Phi(t) = \begin{bmatrix} \alpha_{1s}e^{-\beta_1 t} & \alpha_{1c}e^{-\beta_1 t} & \dots & 0 & 0 \\ \alpha_{1c}e^{-\beta_1 t} & \alpha_{1s}e^{-\beta_1 t} & \dots & 0 & 0 \\ \dots & \dots & \dots & \dots & \dots \\ 0 & 0 & \dots & \alpha_{ms}e^{-\beta_m t} & \alpha_{mc}e^{-\beta_m t} \\ 0 & 0 & \dots & \alpha_{mc}e^{-\beta_m t} & \alpha_{ms}e^{-\beta_m t} \end{bmatrix}$$

(ii) The matrix  $\mathbf{k} \circ \Psi$  in (4) and (5) is also given as the  $2m$ -by- $2m$  sized form such that

$$\mathbf{k}(t) = \begin{bmatrix} \mathbb{1}_{\{C_1(t) < \bar{C}(t)\}} & \mathbb{1}_{\{C_1(t) < \bar{C}(t)\}} & \dots & \mathbb{1}_{\{C_1(t) < \bar{C}(t)\}} & \mathbb{1}_{\{C_1(t) < \bar{C}(t)\}} \\ \mathbb{1}_{\{C_1(t) > \bar{C}(t)\}} & \mathbb{1}_{\{C_1(t) > \bar{C}(t)\}} & \dots & \mathbb{1}_{\{C_1(t) > \bar{C}(t)\}} & \mathbb{1}_{\{C_1(t) > \bar{C}(t)\}} \\ \dots & \dots & \dots & \dots & \dots \\ \mathbb{1}_{\{C_m(t) < \bar{C}(t)\}} & \mathbb{1}_{\{C_m(t) < \bar{C}(t)\}} & \dots & \mathbb{1}_{\{C_m(t) < \bar{C}(t)\}} & \mathbb{1}_{\{C_m(t) < \bar{C}(t)\}} \\ \mathbb{1}_{\{C_m(t) > \bar{C}(t)\}} & \mathbb{1}_{\{C_m(t) > \bar{C}(t)\}} & \dots & \mathbb{1}_{\{C_m(t) > \bar{C}(t)\}} & \mathbb{1}_{\{C_m(t) > \bar{C}(t)\}} \end{bmatrix},$$

where  $\bar{C}(t)$  is given as the average of  $C_i(t)$ 's such as

$$\bar{C}(t) = \frac{C_1(t) + \dots + C_m(t)}{m},$$

and

$$\Psi(t) = \begin{bmatrix} 0 & 0 & \dots & \alpha_{1w}e^{-\beta_1 t} & \alpha_{1n}e^{-\beta_1 t} \\ 0 & 0 & \dots & \alpha_{1n}e^{-\beta_1 t} & \alpha_{1w}e^{-\beta_1 t} \\ \dots & \dots & \dots & \dots & \dots \\ \alpha_{mw}e^{-\beta_m t} & \alpha_{mn}e^{-\beta_m t} & \dots & 0 & 0 \\ \alpha_{mn}e^{-\beta_m t} & \alpha_{mw}e^{-\beta_m t} & \dots & 0 & 0 \end{bmatrix}$$

### 3. Application to Empirical Data

We examine the stylized facts of two major oil-related energy prices in the US. Figure 2 indicates the time series of daily closing prices for WTI crude oil futures and RBOB<sup>8</sup> gasoline futures from 2007 to 2016. Note that the price of gasoline is multiplied by 42 because crude oil price is quoted per barrel, whereas gasoline price is quoted per gallon<sup>9</sup>. Each series is created by connecting the prices of the nearest maturity contracts.

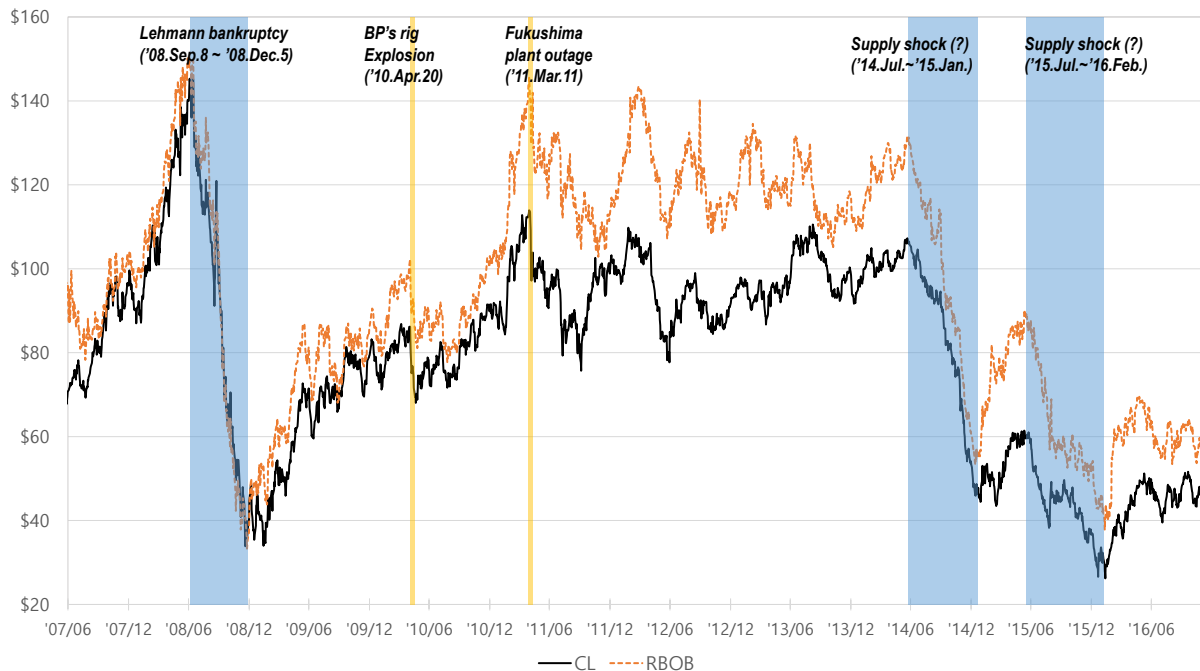


Figure 2: The history of daily closing prices for WTI crude oil futures (CL, black) and RBOB gasoline futures (RB, orange) from January 1, 2007 to December 30, 2016

As shown in Figure 2, there were three big drops in both series: from September 2008 to December 2008; from July 2014 to January 2015; from July 2015 to February 2016. In this section, we investigate the change in parameters of the Hawkes flocking model, especially focusing on the three specified periods when the two prices plunged, and we compare them with the CoVaR values. The data considered in this test are tick size change data in milliseconds for the WTI crude oil and gasoline futures listed in NYMEX from 2007 to 2016.

<sup>8</sup>RBOB stands for reformulated gasoline blendstock for oxygen blending.

<sup>9</sup>1 barrel = 42 gallons

### 3.1. Estimation method

This section explains the ML estimation method we use in this study and demonstrates the simulation to show the ML estimator’s goodness-of-fit to the Hawkes flocking model. The ML method is performed using a likelihood function represented by conditional intensities:

$$\begin{aligned}
 L(\theta) = & \sum_{j=1}^{N_1^u(T)} \log \lambda_1^u(t_{1,j}^u) + \sum_{j=1}^{N_1^d(T)} \log \lambda_1^d(t_{1,j}^d) + \sum_{j=1}^{N_2^u(T)} \log \lambda_2^u(t_{2,j}^u) + \sum_{j=1}^{N_2^d(T)} \log \lambda_2^d(t_{2,j}^d) \\
 & - \int_0^T \left( \lambda_1^u(u) + \lambda_1^d(u) + \lambda_2^u(u) + \lambda_2^d(u) \right) du
 \end{aligned} \tag{9}$$

where  $\lambda_i$  indicates the left-continuous versions of the conditional intensity processes, and  $t_{i,j}$  indicates the associated event times. Parameter  $\theta$  is estimated by maximizing the likelihood function numerically.

Since the estimation proceeds numerically with 12 parameters without the assurance of the convexity of the likelihood function, it is not mathematically guaranteed to find the global maximum. It is therefore worthwhile to check under various situations whether the numerical optimizer can find the correct estimates. Using the present parameters, 500 sample paths are generated for two price processes under the Hawkes flocking model. The presumed values are presented in the column titled “True” in Table 1. The column “Mean” presents the means of the estimates of 500 estimation procedures, which are quite close to the true values. Since the above results show that the numerical optimizer that [Henningesen and Toomet \(2011\)](#) used works well, we apply this procedure in empirical studies.

### 3.2. Data

Data on WTI crude oil and gasoline futures’ trade prices are obtained from the database of Tickdatamarket ([www.tickdatamarket.com](http://www.tickdatamarket.com)). We choose the futures data on “Light Sweet Crude Oil” for WTI crude oil (referred to as “CL” henceforth) and “RBOB Gasoline” for gasoline (referred to as “RB” henceforth) in the energy sector of North America. We consider data for 10 years from January 1, 2007 to December 30, 2016, and each year has 12 delivery months. To construct a single time series over that period for each futures contract, we select data with the nearest delivery month from the observation date, which is usually the most liquid among contracts with maturity longer than one month.

To ensure that raw data can be more feasibly applied to the proposed model, a data wrangling procedure is needed. Without loss of generality, we transform the raw data into a more appropriate format in terms of the following aspects.

(i) *Different price level.*

Table 1: Simulation using ML estimation for a Hawkes flocking model with 500 sample paths

	True	Mean	Std.	True	Mean	Std.	True	Mean	Std.
$\mu_1$	0.0800	0.0803	0.0039	0.0500	0.0503	0.0025	0.1000	0.1000	0.0074
$\alpha_{1n}$	0.0000	-0.0009	0.0124	0.2000	0.2001	0.0206	0.3000	0.3015	0.0324
$\alpha_{1w}$	0.2000	0.2007	0.0142	0.3500	0.3509	0.0200	0.3500	0.3501	0.0247
$\alpha_{1s}$	0.4000	0.4013	0.0083	0.1500	0.1505	0.0140	0.2000	0.1988	0.0176
$\alpha_{1c}$	0.0000	-0.0004	0.0141	0.4000	0.4005	0.0168	0.2000	0.2005	0.0157
$\beta_1$	0.6000	0.6008	0.0212	1.0500	1.0513	0.0368	0.9000	0.9011	0.0402
$\mu_2$	0.0500	0.0500	0.0023	0.0700	0.0702	0.0027	0.1200	0.1207	0.0072
$\alpha_{2n}$	0.0000	-0.0001	0.0105	0.3500	0.3495	0.0269	0.0000	0.0010	0.0215
$\alpha_{2w}$	0.1000	0.1009	0.0115	0.1000	0.1001	0.0162	0.1000	0.1003	0.0216
$\alpha_{2s}$	0.5000	0.5014	0.0242	0.4500	0.4505	0.0213	0.3000	0.2995	0.0224
$\alpha_{2c}$	0.3000	0.3005	0.0178	0.2500	0.2497	0.0142	0.6000	0.6006	0.0282
$\beta_2$	1.2000	1.2028	0.0446	1.3000	1.2999	0.0465	1.1500	1.1519	0.0467

The two futures prices of CL and RB have different price levels. For instance, the CL price at January 13, 2016 with maturity in January 2016 is around \$31, but the RB price is around \$1.07 per gallon, which is \$44.94 per barrel. Minimum tick sizes are also different. The tick size is 0.01 for CL and 0.0001 for RB. Therefore, we need to adjust prices to similar levels. For adjustment, we consider the sample mean ratio,  $\bar{X}/\bar{Y}$  where  $\bar{X}$  implies the sample mean of prices, for example, of the day.

Let  $X$  and  $Y$  be the original price processes. Define  $C_1 = X$ ,  $C_2 = (\bar{X}/\bar{Y})Y$ . However, the adjusted prices on a daily basis are not applicable for the Hawkes flocking model as presented in the left of Figure 3, where  $C_1$  denotes CL and  $C_2$  denotes RB. Data for March 15, 2016 with maturity March 2016 were used. In the early part of the day, it is almost always  $C_1 < C_2$ , but in the later part, it is almost always  $C_2 > C_1$ . Thus, the sample mean should be computed under a shorter time interval. For example, we calculate the sample mean every 10 minutes, and the prices are adjusted during each 10-minute interval. Then the price processes are more applicable, as in the right of Figure 3.

(ii) *Multiple price changes in unit time.*

The minimum resolution time of the data is one second, and multiple price changes can be observed in one second. In this case, we assume that each change occurs at the equi-distant time interval that divides one second with the same number of observations.

(iii) *Simultaneous changes in the two prices.*

The probability that the two prices change at the same time is almost zero in our model,

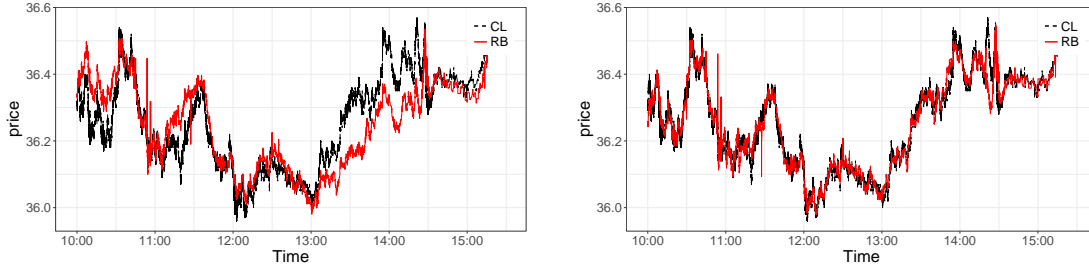


Figure 3: Before (left) and after adjustment (right) for CL and RB prices traded at March 15, 2016

but simultaneous changes in both prices can be recorded in practice. In this case, one price change was assumed to have occurred slightly earlier than the other change. Since this simultaneous jump can be observed several times a day, we consider that one jump to have occurred before the other.

### 3.3. Calibration

From the time series of the CL and RB futures prices after data pre-processing, we estimate the model parameters using the ML estimator presented in Subsection 3.1. The estimation is performed for up to 10 years. We investigate the dynamics of all parameters for the proposed model over time, especially focusing on the periods of plunges in the CL and RB prices.

#### *Robustness test for the Hawkes flocking model parameters*

Before implementing model calibration, we conduct a test for the relation between the two parts in the intensity kernel  $\mathbf{h}$ : a self- and mutually-excited factor and a flocking factor. We consider two models with different kernels: (i) a symmetric Hawkes model without a flocking term versus (ii) a Hawkes flocking model. Then, we compare the parameter estimation results derived from each model.

First, we assume that CL and RB futures prices follow a symmetric Hawkes process that has an exponential decaying kernel without a flocking term, that is

$$\lambda_t = \boldsymbol{\mu} + \int_{-\infty}^t \boldsymbol{\Phi}(t-u) d\mathbf{N}_u \quad (10)$$

where the matrix  $\boldsymbol{\Phi}$  is symmetric with parameters  $\alpha_{is}$ ,  $\alpha_{ic}$ , and  $\beta_i$  for  $i = 1, 2$ , as defined in (3). In this setup, since the flocking phenomenon between the CL and RB futures prices is not implicated, the two processes are independent.

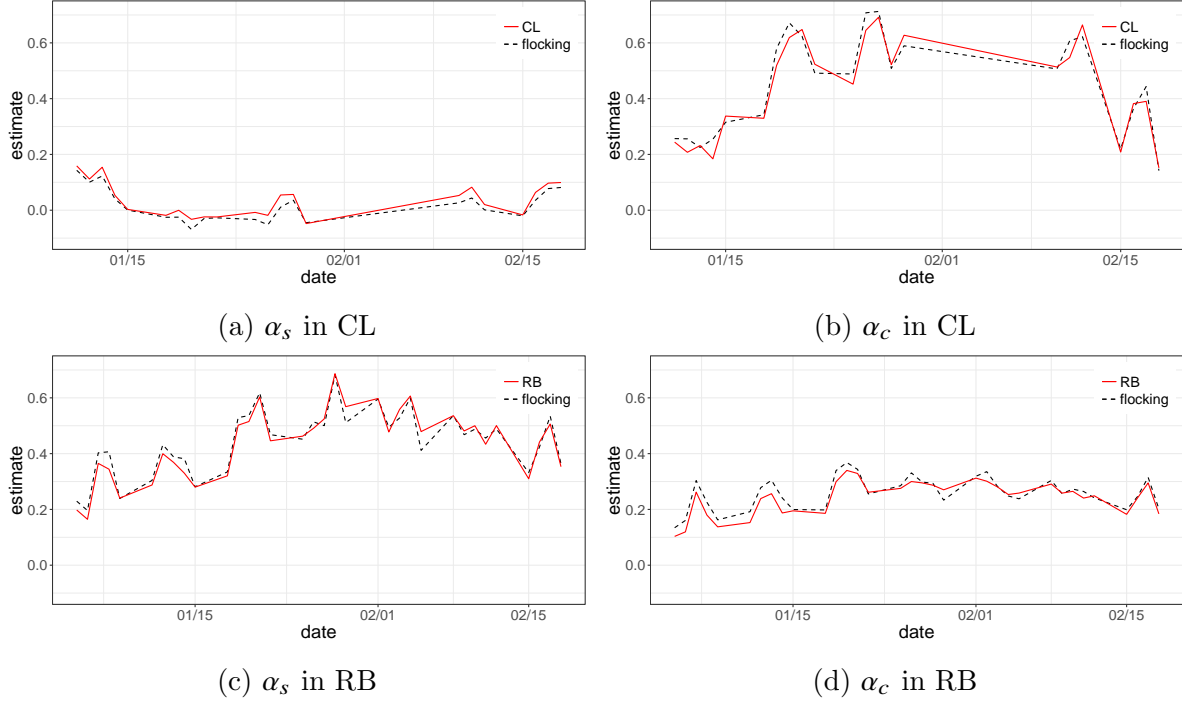


Figure 4: Comparison of estimates of  $\alpha_s$  and  $\alpha_c$  under a symmetric Hawkes model (red solid line) and the Hawkes flocking model (black dotted line) for CL and RB futures prices with maturity in February 2016 from January 4 to February 22, 2016

Second, we assume that CL and RB futures prices follow the Hawkes flocking process, that is,

$$\lambda_t = \boldsymbol{\mu} + \int_{-\infty}^t \boldsymbol{\Phi}(t-u) + \mathbf{k}(u) \circ \boldsymbol{\Psi}(t-u) d\mathbf{N}_u \quad (11)$$

where the matrix  $\mathbf{k}$  and  $\boldsymbol{\Psi}$  are defined in (4) and (5), respectively, with additional parameters  $\alpha_{in}, \alpha_{iw}$  for  $i = 1, 2$ .

**Example 1.** [*Multicollinearity for  $\alpha_s$  and  $\alpha_c$* ]. We estimated the parameters  $\alpha_s$  and  $\alpha_c$  from CL and RB futures prices under each model assumption. The test is performed on a daily basis on the futures prices with maturity in February 2016, and the observation period is from January 4 to February 22, 2016. Figure 4 illustrates the results of  $\alpha_s$  and  $\alpha_c$  for CL and RB under the symmetric Hawkes model (red solid line) and the Hawkes flocking model (black dashed line).

We find that the estimates under different model assumptions are almost identical over the observed period. This implies that  $\mathbf{k}(u) \circ \boldsymbol{\Psi}(t-u)$  in the Hawkes flocking model does not affect the existing self- and mutually-exciting parts  $\boldsymbol{\Phi}(t-u)$ . This concept can be considered as being similar to the non-existence of multicollinearity in linear regression.

**Example 2.** [*Multicollinearity for  $\mu$  and  $\beta$* ]. We conducted the same test as in Example 1 on the base intensity parameter  $\mu_i$  and the resilience speed to the base intensity  $\beta_i$  over the same sample period. Figures 5 and 6 show the results of parameters  $\mu_i$  and  $\beta_i$  based on the two models, respectively.

For  $\mu$ , we find that both CL and RB futures prices of the symmetric Hawkes model have larger  $\mu$  than those of the Hawkes flocking model. The reason is that additional fluctuations in price processes due to the flocking phenomenon are considered as a part of exogenous dynamics, and hence they are inherent to  $\mu$  under the symmetric Hawkes models where flocking terms,  $\alpha_n$  and  $\alpha_w$ , do not exist.

For  $\beta$ , we see that results from the symmetric Hawkes and Hawkes flocking models are very similar for the CL futures price. Meanwhile, the  $\beta$  in the Hawkes flocking model is slightly larger than  $\beta$  in the symmetric Hawkes model for the RB futures price. This implies that “ $\beta$  due to  $\alpha_n$ ” and  $\alpha_w$  is larger than “ $\beta$  due to  $\alpha_s$ ” and  $\alpha_c$  in RB. Note that a large  $\beta$  implies weak persistence. We do not rule the possibility out that  $\beta$  depends on  $\alpha$ 's but merely consider unified  $\beta$  for model parsimony.

**Example 3.** [*Significance of  $\alpha_n$  and  $\alpha_w$* ]. Figure 7 compares  $\alpha_n$  and  $\alpha_w$  under the Hawkes flocking model over the same sample period. In particular, the narrowing events' parameters  $\alpha_{in}$  are depicted with plus minus two times of standard errors (dotted lines) to check the significance of the estimates. The result shows that  $\alpha_{in}$  are close to zero in the selected time period and this means that the price difference of narrowing events does not substantially affect the intensities. This is quite intuitive.

On the other hand,  $\alpha_{iw}$  are significant. This means that the widening event significantly increases intensities associated with the flocking so that the two price processes tend to converge toward each other after widening events. The standard errors of  $\alpha_{iw}$  are omitted for clarity of the graph but the estimates of  $\alpha_{iw}$  are statistically significant for all time period. For the graph, selected maturity for the futures is in February 2016 and estimates are computed on a daily basis. In addition,  $\alpha_w$  in CL is larger than that in RB.

More relevant examples for other sample periods appear in Appendix C.

#### *Dynamics of estimates over the past decade*

Based on the argument of the robustness check, we calibrate the Hawkes flocking model by expanding the test period from a sample month (February 2016) to the recent decade from January 2007 to December 2016. Using the transaction data of CL and RB futures prices, the estimates are computed on a daily basis and the daily estimates are averaged over a month for better visualization. The associated results are displayed in Figures 8, 9, and 10.

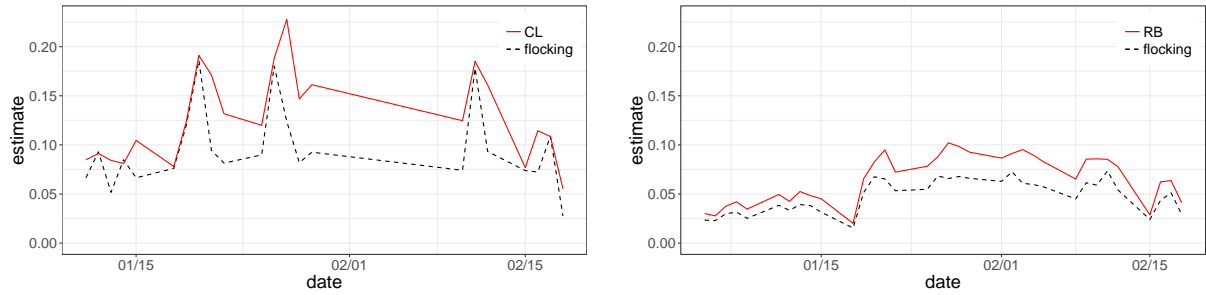


Figure 5: Comparison of estimates of  $\mu_1$  and  $\mu_2$  under the symmetric Hawkes model (red line) and the Hawkes flocking model (black dotted line) for CL and RB futures prices with maturity in February 2016 from January 4 to February 22, 2016

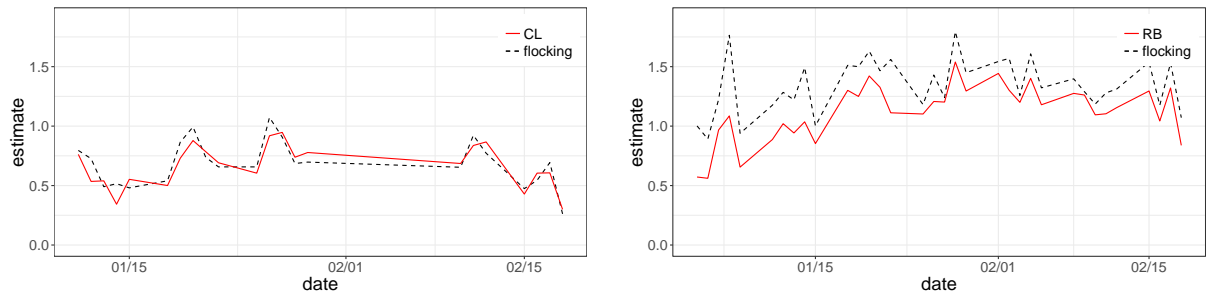


Figure 6: Comparison of estimates of  $\beta_1$  and  $\beta_2$  under the symmetric Hawkes model (red line) and the Hawkes flocking model (black dotted line) for CL and RB futures prices with maturity in February 2016 from January 4 to February 22, 2016

Figure 8 exhibits the flocking parameters  $\alpha_n$  (red solid line) and  $\alpha_w$  (black dotted line) for CL futures (left panel) and RB futures (right panel). For each futures price, the level of  $\alpha_n$  is much smaller than that of  $\alpha_w$  and it is close to zero for a long time period. This seems reasonable because widening events have a strong role causing the flocking phenomenon, while narrowing events have no or relatively small effects. In CL,  $\alpha_w$  has the maximum value near the fourth quarter of 2008, and it gradually decreases and then increases again around 2015. In RB,  $\alpha_w$  gradually increases.

Figure 9 shows the behavior of  $\alpha_s$  (black dotted line) and  $\alpha_c$  (red solid line) for CL futures (left panel) and RB futures (right panel). The self-exciting parameter  $\alpha_s$  in CL gradually decreases over time and is close to zero in 2016. All other parameters are far from zero and do not show any particular trend. In general,  $\alpha_c$  is greater than  $\alpha_s$  in CL and  $\alpha_c$  is less than  $\alpha_s$  in RB over the sample period. It is known that the self-exciting pattern is due to order splitting and the mutually-exciting pattern is due to microstructure noise.

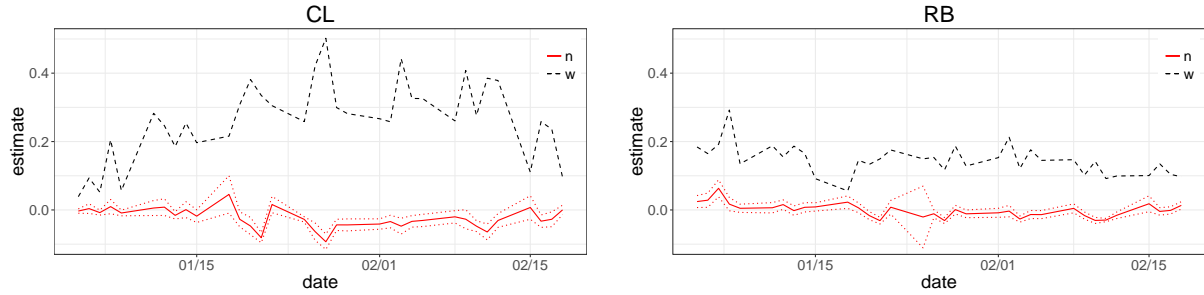


Figure 7: Comparison of  $\alpha_n$  and  $\alpha_w$  for CL (left) and RB (right) futures prices with maturity in February 2016 from January 4 to February 22, 2016

Figure 10 plots the behavior of exogenous fluctuation parameter  $\mu$  (left panel) and persistence parameter  $\beta$  (right panel). As mentioned before, the dynamics of  $\mu$  seem related to the dynamics of  $\alpha_w$ . In general,  $\mu$  in CL is larger than RB but the gap is closing. Meanwhile, the persistence parameter  $\beta$  is smaller in CL, and this implies that persistence in CL is stronger than in RB. In addition, there is no particular trend in  $\beta$ .

#### *Interpretation of the estimation results*

We observe that the main source for the convergence of the two price processes is CL by the fact that  $\alpha_w$  in CL is greater than  $\alpha_w$  in RB. As shown in the left of Figure 11, when the CL price is larger than the RB price, dropping RB price is a widening event. In this case, the narrowing tendency can be facilitated by (i) increase of the up intensity in RB or (ii) increase of the down intensity in CL. Increase of the up intensity in RB price is represented by  $\alpha_c$  in RB, since it is caused by the previous downward movement in RB. This is captured by the individual Hawkes price model within the RB futures price. Increase of the down intensity in CL is represented by  $\alpha_w$  in CL, since it is caused by a widening event affecting the intensity of CL. This is captured by the Hawkes flocking model, which explains the interaction between the CL and RB futures prices.

When we compare  $\alpha_c$  in RB and  $\alpha_w$  in CL in Figures 8 and 9, generally  $\alpha_w$  in CL are larger than  $\alpha_c$  in RB. Although this does not strictly imply that the two price paths are more likely to be narrowed by CL, we deduce that the influence of CL on narrowing is quite significant.

Similarly, when CL is greater than RB, as in the right of Figure 11, increasing CL implies a widening event. As before, the narrowing tendency can be facilitated by (i) increase of the up intensity in RB or (ii) increase of the down intensity in CL. Increase of the up intensity in RB is represented by  $\alpha_w$  in RB, since it is caused by a widening event affecting the intensity of RB. The increase of the down intensity in CL is represented by

$\alpha_c$  in CL, since it is caused by an upward movement of CL.

When we compare  $\alpha_w$  in RB and  $\alpha_c$  in CL in Figures 8 and 9, generally,  $\alpha_c$  in CL are much larger than  $\alpha_w$  in RB. This means that if the two price paths are widened, then the tendency to converge toward each other increases for both prices, but the increment is much more significant in CL than in RB. We can deduce that, in many cases, the flocking feature between CL and RB is more likely to be owing to CL.

One possible interpretation of this result is that participants in WTI crude oil futures market seem to use information from the gasoline market more actively than do participants in the gasoline futures market from the WTI crude oil futures market.

#### 4. Comparison with a Systemic Risk Measure

In this section, we compare the levels of the systemic risk embedded in the two futures prices that are (i) obtained by branch ratios in our proposed model and (ii) measured by CoVaR. To do so, we adopt a CoVaR-copula approach, which is developed by [Reboredo and Ugolini \(2015\)](#) and [Reboredo \(2015\)](#), to the empirical data of WTI crude oil and gasoline futures prices.

##### 4.1. A CoVaR-copula approach

CoVaR is a most widely used systemic risk measure, proposed by [Adrian and Brunnermeier \(2016\)](#), with systemic expected shortfall and SRISK that measures the capital shortfall (see [Acharya et al., 2017](#); [Brownlees and Engle, 2017](#)). The systemic risk measures focus on a spillover effect from one to another.

The CoVaR is the VaR for the financial system conditional on the fact that an individual financial institution is under stress. Let  $R_t^i$  be the return for the financial market as a whole at time  $t$  and let  $R_t^j$  be the return for market  $j$  at time  $t$ . The original definition of CoVaR is given by

$$\mathbb{P}\left(R_t^i \leq \text{CoVaR}_{\beta,t}^{i|j,\alpha=q} | R_t^j = \text{VaR}_{q,t}^j\right) = \beta. \quad (12)$$

This is the VaR when the return of market  $j$  stands at the VaR with the  $q$ -percent confidence level. After that, by replacing the condition to make it more realistic, the definition was extended to the following form.

$$\mathbb{P}\left(R_t^i \leq \text{CoVaR}_{\beta,t}^{i|j} | R_t^j \leq \text{VaR}_{\alpha,t}^j\right) = \beta, \quad (13)$$

where  $\text{VaR}_{\alpha,t}^j$  is the VaR for market  $j$ , measuring the maximum loss that market  $j$  may experience for confidence level  $1 - \alpha$  and a specific time horizon, that is, the  $\alpha$ -quantile of the return distribution for the market  $j$ :  $\mathbb{P}(R_t^j \leq \text{VaR}_{\alpha,t}^j) = \alpha$ .

Using the CoVaR, the systemic risk can be measured by the delta CoVaR ( $\Delta\text{CoVaR}$ ), which is the difference between the VaR of whole market conditional on the distressed state of market  $j$ , that is,  $R_t^j \leq \text{VaR}_{\alpha,t}^j$ , and the VaR of the the whole market conditional on the normal state of market  $j$ , that is,  $R_t^j = \text{VaR}_{\alpha=50\%,t}^j$ . Note that usually the median quantile is considered.

To implement the defined  $\Delta\text{CoVaR}$  as presented, we consider a copula function approach to implement  $\Delta\text{CoVaR}$ . By consolidating the definition of CoVaR proposed by the relevant literature, we present the formula as an analytic form using a copula function. The following proposition shows the formula for computing  $\Delta\text{CoVaR}$  with the relevant proof in Appendix B.

**Proposition 4.** For a uniform vector  $(U, V)$  with a copula function  $C$ , let  $h_v(u)$  denote the conditional distribution by

$$h_v(u) = \mathbb{P}(U \leq u | V = v) = \frac{\partial C(u, v)}{\partial v}, \quad (14)$$

and  $C_\alpha^{-1}(\cdot)$  denote the inverse of  $C_\alpha : x \rightarrow C(\cdot, \alpha)$ . Then, the  $\beta$ -quantile  $\Delta\text{CoVaR}_t^{ij}$  of asset  $i$ 's return  $R^i$  conditional on asset  $j$ 's return  $R^j$  is given as an analytic form:

$$\Delta\text{CoVaR}_t^{ij} = \text{CoVaR}_{\beta,t}^{ij} - \text{CoVaR}_{\beta,t}^{ij,\alpha=0.5}. \quad (15)$$

Each part of (15) is computed by

$$\text{CoVaR}_{\beta,t}^{ij} = F_{R_t^i}^{-1} \left( C_\alpha^{-1}(\alpha\beta) \right) \quad \text{and} \quad \text{CoVaR}_{\beta,t}^{ij,\alpha=q} = F_{R_t^i}^{-1} \left( h_q^{-1}(\beta) \right), \quad (16)$$

where  $F_{R_t^i}$  is the marginal distribution function of  $R_t^i$ .

To apply the notion of  $\Delta\text{CoVaR}$  to our study, we compute it based on daily returns for two price dynamics. This measure captures the level of systemic risk in a day. We replicate the computation presented in Proposition 4 to the transaction data over a regular time stamp  $t$ .

Let  $R_t^1$  and  $R_t^2$  be the returns for daily observations of  $C_1(t)$  and  $C_2(t)$ , respectively, that is,

$$R_t^1 = \frac{C_1(t + \Delta t) - C_1(t)}{C_1(t)}, \quad R_t^2 = \frac{C_2(t + \Delta t) - C_2(t)}{C_2(t)}, \quad (17)$$

where  $\Delta t$  is given by a one-day length.

We consider the following 4 copulas with different tail dependencies and symmetries: the Gaussian copula with tail independence; Student  $t$  copula with symmetric tail dependence; Gumbel copula with upper tail dependence and lower tail independence; Clayton copula with upper tail independence and lower tail dependence. The details are specified in Table 2. Appendix A presents how to implement time-varying CoVaR using the copula functions.

Copula	Distribution $C(u, v; \cdot)$	Range of $\theta$	$\lambda_L$	$\lambda_U$	Generator $\psi(\cdot)$
Gaussian	$\Phi_\theta(\Phi^{-1}(u), \Phi^{-1}(v))$	$(-1, 1)$	0	0	$\times$
Student $t$	$T_{v,\theta}(t_v^{-1}(u), t_v^{-1}(v))$	$(-1, 1)$	$2t_{v+1}$	$\left(-\frac{\sqrt{v+1}\sqrt{1-\theta}}{\sqrt{1+\theta}}\right)$	$\times$
Gumbel	$\exp\left(-[(\ln u)^\theta + (\ln v)^\theta]^{1/\theta}\right)$	$[1, \infty)$	0	$2 - 2^{1/\theta}$	$(-\ln t)^\theta$
Clayton	$(u^{-\theta} + v^{-\theta} - 1)^{-\frac{1}{\theta}}$	$(0, \infty)$	$2 - 2^{1/\theta}$	0	$(t^{-\theta} - 1)/\theta$

Table 2: Bivariate copula models with correlation parameter  $\theta$ , upper tail dependence  $\lambda_L$ , lower tail  $\lambda_U$  dependence parameters

#### 4.2. Level of systemic risk

Let  $R_t^1$  and  $R_t^2$  be same as defined in (17) by the daily returns of CL and RB futures prices, respectively. We compute one-day  $\Delta\text{CoVaR}_t^{1|2}$  and one-day  $\Delta\text{CoVaR}_t^{2|1}$  based on  $R_t^1, R_t^{2|10}$ . The value of one-day  $\Delta\text{CoVaR}_t^{1|2}$  is interpreted as the extent to which extreme downward changes in gasoline futures price (conditioned variable) contribute to the systemic risk in WTI crude oil futures price for a day at time  $t$ . Conversely, the value of  $\Delta\text{CoVaR}_t^{2|1}$  indicates the contribution of extreme downward changes in WTI crude oil futures price (conditioned variable) to systemic risk in gasoline futures price.

#### Selection of the best fitting copula

We estimated marginal distributions for each return series of CL and RB futures prices using the ARMA(1,1)-TGARCH(1,1) model with skewed- $t$  distribution. Then, we transformed the daily return series into uniform variables such that  $\hat{u}_t = \hat{F}_1(x_t)$  and  $\hat{v}_t = \hat{F}_2(y_t)$  where  $\hat{F}_i$  is the estimated distribution and  $x_t, y_t$  are the standardized returns of  $R_t^1, R_t^2$ , respectively. Figure 12 displays the scatter plot of 2,000 days of pseudo-sample observations,  $\hat{u}_t, \hat{v}_t$  under the marginal distribution model.

We extracted dependence parameters of the copula functions reported in Table 2 using the consecutive  $d$  days of series pairs. Figure 18 (Appendix D) illustrates the dynamics of the estimated parameter  $\theta$  of CL and RB futures prices using given copulas with the standard error during the test period from 2007 to 2016.

To select the best fitting copula among them, we compare different copula specifications using the commonly used error measures of Akaike information criterion (AIC) and Bayesian information criterion (BIC) in the model selection based on an ML estimation.

<sup>10</sup>Since profit returns (not loss returns) are used in the computation of CoVaR and VaR, the CoVaR and VaR values with the minus sign are considered throughout the test. The minus VaR is usually given as a positive value when the quantile level is greater than 50%.

Figure 13 shows the results of AIC and BIC values from estimations of the Gaussian, Student  $t$ , Gumbel, and Clayton copulas over time. We find that the Student  $t$  copula provides the lowest values by both measures on the entire timeline.

In addition, the degrees of freedom  $\nu$  for the Student  $t$  copula are estimated over time and displayed in Figure 19 (Appendix D), which provides evidence of fat tails of the joint distribution of the return pair of CL and RB futures prices. The empirical result indicates the existence of positive and symmetric dependence with fat tails between the two futures prices. The extent of the overall positive dependency and extreme tail dependency has varied over time.

#### *Computation of CoVaRs*

By taking the best fitting copula obtained above, we computed time-varying  $\text{CoVaR}_t$  using Proposition 4 with an analytic form of the  $h_\alpha$  function. Since the Student  $t$  copula was chosen as having the best fit to our data over the whole test period by the AIC and BIC tests, function (24) was employed only in our analysis. We picked the 95% quantile level for computing the CoVaR and VaR used in the conditioned part of CoVaR, that is,  $\alpha = 5\%$  and  $\beta = 5\%$ .

Figure 20 (Appendix D) shows the dynamics of one-day 95%  $\text{CoVaR}_t^{1|2}$  and  $\text{CoVaR}_t^{2|1}$  when the conditional variable is given as the distressed situation and when it is given as the normal situation  $\alpha = 50\%$  as presented in (12) and (13), respectively, from 2007 to 2016. The shaded areas represent the three large drops in the WTI crude oil and gasoline futures prices as mentioned in Figure 2. We find that both CoVaR and  $\Delta\text{CoVaR}$  values significantly increase in distressed time periods compared with other normal times. Moreover, relative contributions of the WTI crude oil futures to the systemic risk in gasoline futures, and vice versa, changed almost similarly over time.

#### *4.3. Comparison between branch ratios and system risk measures*

In Section 2, we derived the spectral radius  $\rho_{\mathbf{M}}$  of the branch matrix  $\mathbf{M}$  for the Hawkes flocking model. Applying the definition of  $\rho_{\mathbf{M}}$  to the framework of our empirical study, it can be naturally interpreted as the maximum level of instability, that is, systemic risk, that exists within and between high-frequency markets of WTI crude oil and gasoline futures.

#### *Levels of endogeneity and interaction*

As discussed earlier, branch matrix  $\mathbf{M}$  is of four-by-four size that contains 16 compo-

nents as follows.

$$\mathbf{M} = \begin{bmatrix} \frac{\alpha_{1s}}{\beta_1} & \frac{\alpha_{1c}}{\beta_1} & \frac{\alpha_{1w}}{2\beta_1} & \frac{\alpha_{1n}}{2\beta_1} \\ \frac{\alpha_{1c}}{\beta_1} & \frac{\alpha_{1s}}{\beta_1} & \frac{\alpha_{1n}}{2\beta_1} & \frac{\alpha_{1w}}{2\beta_1} \\ \frac{\alpha_{2w}}{2\beta_2} & \frac{\alpha_{2n}}{2\beta_2} & \frac{\alpha_{2s}}{\beta_2} & \frac{\alpha_{2c}}{\beta_2} \\ \frac{\alpha_{2n}}{2\beta_2} & \frac{\alpha_{2w}}{2\beta_2} & \frac{\alpha_{2c}}{\beta_2} & \frac{\alpha_{2s}}{\beta_2} \end{bmatrix} \quad (18)$$

Matrix  $\mathbf{M}$  can be divided by a four distinct quadrants (indicated by dash lines) according to the role of parameters, as shown in (18). The components in the first and fourth quadrants represent the branch ratios that affect the self- and mutually-exciting factors in CL and RB price processes, respectively. Similarly, the components in the second and third quadrants represent the branch ratios that affect the flocking feature (widening and narrowing events) in CL and RB price processes, respectively.

To capture the different patterns of dynamics in terms of the self- and mutually-exciting factors as well as flocking factors explained by  $\alpha_{is}, \alpha_{ic}$  and  $\alpha_{in}, \alpha_{iw}$ , respectively, we examine the branch ratios by component. By taking the average of the four components belonging to each quadrant, we consider the following branch ratios.

$$\frac{\alpha_{1s} + \alpha_{1c}}{\beta_1}, \quad \frac{\alpha_{2s} + \alpha_{2c}}{\beta_2}, \quad \frac{\alpha_{1n} + \alpha_{1w}}{2\beta_1}, \quad \frac{\alpha_{2n} + \alpha_{2w}}{2\beta_2}. \quad (19)$$

Each value has the following interpretation:

- (i)  $(\alpha_{is} + \alpha_{ic})/\beta_i$  indicates the average frequency of the occurrence of offspring events due to price upward or downward movements per one exogenous event that comes into each CL or RB futures price, for  $i = 1, 2$ . This can be interpreted as *the level of endogeneity* that exists in WTI crude oil futures market for  $i = 1$  and gasoline future market for  $i = 2$ .
- (ii)  $(\alpha_{in} + \alpha_{iw})/(2\beta_i)$  corresponds to the average frequency of the occurrence of offspring events due to widening and narrowing events between the two prices per one exogenous event that comes into the each futures price. This can be interpreted as *the level of risk interaction* from gasoline to WTI crude oil futures markets for  $i = 1$  and the opposite direction for  $i = 2$ .

#### *Illustration of the level of systemic risk with benchmark measures*

We simulate the spectral radius in (7) and the branch ratios specified in (19) using the best fitting kernel parameters  $\alpha_{is}, \alpha_{ic}, \alpha_{in}, \alpha_{iw}$ , and  $\beta_i$  for  $i = 1, 2$  in the Hawkes flocking model with  $p = 1/2$ , as discussed in Subsection 3.3. Moreover, the branch ratios are compared with VaR and CoVaR as a benchmark of the systemic risk. The relevant results are displayed in Figures 14, 15, and 16.

Figure 14 illustrates the evolution of the spectral radius of the branch matrix  $\mathbf{M}$ . We observe that mid-2008 had the highest level of spectral radius at around 85% just before the collapse of Lehman Brothers in September 2008. With the onset of the global credit crisis, the overall level decreased until the beginning of 2011 when it was the lowest at around 63% during the test period up to December 2016.

Figure 15 presents the evolution of the branch ratios  $(\alpha_{1s} + \alpha_{1c})/\beta_1$  for CL futures,  $(\alpha_{2s} + \alpha_{2c})/\beta_2$  for RB futures and their one-day 95% VaR values from January 2007 to December 2016. For the CL futures, the branch ratio varies between 58% and 82%; however, for RB futures, it varies between 32% and 60%. This implies that the level of endogeneity in CL futures market was consistently higher than that in RB futures prices for the past decade. In CL futures in mid-2008, the highest level of endogeneity was recorded just before the onset of the global crisis. Meanwhile, there were no significant changes for this level in the second and third plunge periods in the CL and RB markets in 2014 and 2016, respectively. On the other hand, for one-day 95% VaR values, precipitous rises occurred on mid-2008, 2014, and 2016 in both CL and RB markets, and the overall flows of VaR in CL and RB markets were similar.

Figure 16 presents the evolution of the branch ratios  $(\alpha_{1n} + \alpha_{1w})/2\beta_1$  for the CL process affected by the RB price fluctuation,  $(\alpha_{2n} + \alpha_{2w})/2\beta_2$  for the RB process affected by CL price fluctuation, and one-day 95%  $\Delta\text{CoVaR}_t^{1|2}$  and  $\Delta\text{CoVaR}_t^{2|1}$  from January 2007 to December 2016. At a microscopic level, the degree to which RB affects CL has values ranging between 10% and 55%; however, the degree to which CL affects RB is between 2% and 8%. This means that the level to which RB price affects CL price has been consistently higher than that in its opposite direction over the past 10 years. Moreover, a reverse pattern was observed between the relative influences on the two high-frequency price processes. For the degree of the impact of the change in RB price on CL price, the highest level was recorded in late 2008, it gradually decreased after that but rose slightly during the second and third plunge periods. On the other hand, the level to which the CL price affects RB price was the lowest in late 2008, but it increased to the highest level during the second and third plunge periods. For delta CoVaR values, the extent of their relative contribution to systemic risk due to each futures market was almost symmetric.

Throughout the test, we uncover some remarkable facts about the futures markets of WTI crude oil and gasoline in terms of high-frequency structure. First, the overall systemic risk level in the two futures markets was the highest before the onset of the global credit crisis, and there was no considerable change in overall systemic risk in these markets when the price plunges occurred in 2014 and 2016. Second, when we compare the levels of endogeneity embedded in each futures market, the level of the WTI market was

a significantly higher than that in the gasoline market. Moreover, since the WTI crude oil market is more actively affected by change in the gasoline market, it is more likely to react promptly to a delicate change in the gasoline market than in the opposite case. Last, the levels of the risk interaction between the two markets, that is, from WTI crude oil to gasoline and vice versa, were very asymmetric. However, the degree of the difference has been reducing steadily over the past decade.

## 5. Concluding Remark

We propose a Hawkes flocking model to quantify systemic risk in high-frequency markets. The model is designed to capture self- and mutually-exciting features as well as cross-exciting on the intensity processes depending on the relative position of asset prices as the price difference is narrowed or widened. In the empirical study, we observe a micro-level behavior between the two futures markets of WTI crude oil and gasoline. We see that when the difference of the two prices narrows, no additional flocking phenomenon occurs, but, when they get widened, a strong flocking phenomenon occurred. The Hawkes flocking model-based assessment is highly suitable for application of tick-by-tick data, and it is also feasible to capture a delicate change in the level of system risk that appears in highly correlated data.

In terms of the assessment of systemic risk, we compare the results of the branch ratios derived from the Hawkes flocking model with the delta CoVaR, which is introduced as a benchmark for the proposed metric of the systemic risk. Estimating the best fit kernel using a ML estimator from the given data set, we obtain the following empirical results. The systemic risk level in the WTI crude oil futures price has been consistently higher than that in the gasoline futures price for the test period. Furthermore, the change in gasoline futures price has a significantly greater impact on WTI crude oil futures price than in the opposite case, which implies that the relative contribution of each price is asymmetric at the microscopic level of price structure.

## Acknowledgements

This work was supported by the National Research Foundation of Korea (NRF) grant funded by the Korea government (MSIT) (No.2017R1C1B5074398); and the National Research Foundation of Korea(NRF) grant funded by the Korea government(MSIT) (No.2017R1C1B5017338).

## References

- Aas, K., Czado, C., Frigessi, A., and Bakken, H. (2009). Pair-copula constructions of multiple dependence. *Insurance: Mathematics and Economics*, 44(2):182–198.
- Acharya, V. V., Pedersen, L. H., Philippon, T., and Richardson, M. (2017). Measuring systemic risk. *The Review of Financial Studies*, 30(1):2–47.
- Adrian, T. and Brunnermeier, M. K. (2016). Covar. *American Economic Review*, 106(7):1705–41.
- Bacry, E., Dayri, K., and Muzy, J.-F. (2012). Non-parametric kernel estimation for symmetric hawkes processes. application to high frequency financial data. *The European Physical Journal B*, 85(5):157.
- Bacry, E., Delattre, S., Hoffmann, M., and Muzy, J.-F. (2013). Modelling microstructure noise with mutually exciting point processes. *Quantitative Finance*, 13(1):65–77.
- Bacry, E., Mastromatteo, I., and Muzy, J.-F. (2015). Hawkes processes in finance. *Market Microstructure and Liquidity*, 1(01):1550005.
- Bormetti, G., Calcagnile, L. M., Treccani, M., Corsi, F., Marmi, S., and Lillo, F. (2015). Modelling systemic price cojumps with hawkes factor models. *Quantitative Finance*, 15(7):1137–1156.
- Bowsher, C.-G. (2007). Modelling security market events in continuous time: Intensity based, multivariate point process models. *Journal of Econometrics*, 141(2):876–912.
- Brownlees, C. and Engle, R.-F. (2017). Srisk: A conditional capital shortfall measure of systemic risk. *The Review of Financial Studies*, 30(1):48–79.
- Calcagnile, L.-M., Bormetti, G., Treccani, M., Marmi, S., and Lillo, F. (2018). Collective synchronization and high frequency systemic instabilities in financial markets. *Quantitative Finance*, 18:237–247.
- Chavez-Demoulin, V. and McGill, J. (2012). High-frequency financial data modeling using hawkes processes. *Journal of Banking & Finance*, 36(12):3415–3426.
- Chiu, M. C., Wong, H. Y., and Zhao, J. (2015). Commodity derivatives pricing with cointegration and stochastic covariances. *European Journal of Operational Research*, 246(2):476–486.

- Da Fonseca, J. and Zaatour, R. (2014). Hawkes process: Fast calibration, application to trade clustering, and diffusive limit. *Journal of Futures Market*, 34(6):548–579.
- Danielsson, J., Shin, H. S., and Zigrand, J.-P. (2012). Endogenous and systemic risk. In *Quantifying systemic risk*, pages 73–94. University of Chicago Press.
- Fang, F., Sun, Y., and Spiliopoulos, K. (2017). On the effect of heterogeneity on flocking behavior and systemic risk. *Statistics & Risk Modeling*, 34(3-4):–.
- Fernández, C. and Steel, M. F. (1998). On bayesian modeling of fat tails and skewness. *Journal of the American Statistical Association*, 93(441):359–371.
- Filimonov, V. and Sornette, D. (2012). Quantifying reflexivity in financial markets: Toward a prediction of flash crashes. *Physical Review E*, 85(5):056108.
- Girardi, G. and Ergun, A.-T. (2013). Systemic risk measurement: Multivariate garch estimation of covar. *Journal of Banking and Finance*, 37(11):3169–3180.
- Granger, C. W. (1981). Some properties of time series data and their use in econometric model specification. *Journal of econometrics*, 16(1):121–130.
- Ha, S.-Y., Kim, K.-K., and Lee, K. (2015). A mathematical model for multi-name credit based on community flocking. *Quantitative Finance*, 15(5):841–851.
- Hardiman, S. J., Bercot, N., and Bouchaud, J.-P. (2013). Critical reflexivity in financial markets: a hawkes process analysis. *The European Physical Journal B*, 86(10):442.
- Hawkes, A. G. (1971a). Point spectra of some mutually exciting point processes. *Journal of the Royal Statistical Society. Series B (Methodological)*, 33(3):438–443.
- Hawkes, A. G. (1971b). Spectra of some self-exciting and mutually exciting point processes. *Biometrika*, 58(1):83–90.
- Hawkes, A. G. and Oakes, D. (1974). A cluster process representation of a self-exciting process. *Journal of Applied Probability*, 11(3):493–503.
- Henningsen, A. and Toomet, O. (2011). maxlik: A package for maximum likelihood estimation in r. *Computational Statistics*, 26(3):443–458.
- Jain, P. K., Jain, P., and McInish, T. H. (2016). Does high-frequency trading increase systemic risk? *Journal of Financial Markets*, 31:1–24.

- Lee, K. and Seo, B.-K. (2017). Modeling microstructure price dynamics with symmetric hawkes and diffusion model using ultra-high-frequency stock data. *Journal of Economic Dynamics and Control*, 79(6):154–183.
- Miller, R.-S. and Shorter, G. (2016). High frequency trading: Overview of recent developments. *Congressional Research Service*.
- Reboredo, J. C. (2015). Is there dependence and systemic risk between oil and renewable energy stock prices? *Energy Economics*, 48:32–45.
- Reboredo, J. C. and Ugolini, A. (2015). Systemic risk in european sovereign debt markets: A covar-copula approach. *Journal of International Money and Finance*, 51:214–244.
- Schepsmeier, U. and Stöber, J. (2014). Derivatives and fisher information of bivariate copulas. *Statistical Papers*, 55(2):525–542.

## A. A CoVaR-Copula Approach

Under the copula specifications in Table 2, we follow a three-step procedure to implement the time-varying CoVaR.

*Step 1. Estimating marginal distributions for returns.*

To estimate the marginal distributions for each return  $R_t^\ell$  for  $\ell = 1, 2$ , we use an ARMA( $p, q$ ) – TGARCH( $r, m$ ) model, that is,

$$R_t = \phi_0 + \sum_{j=1}^p \phi_j R_{t-j} + \epsilon_t - \sum_{i=1}^q \theta_i \epsilon_{t-i}, \quad (20)$$

where  $p$  and  $q$  are non-negative integers and  $\phi$  and  $\theta$  are the ARMA parameters, respectively. Here,  $\epsilon_t = \sigma_t z_t$ , and  $\sigma_t^2$  is the conditional variance given by a TGARCH specification:

$$\sigma_t^2 = \omega + \sum_{k=1}^r \beta \sigma_{t-k}^2 + \sum_{h=1}^m \alpha_h \epsilon_{t-h}^2 + \sum_{h=1}^m \lambda_h \epsilon_{t-h}^2 \mathbb{1}_{\{t-h>0\}}, \quad (21)$$

where  $\omega$  is a constant,  $\sigma_{t-k}^2$  is the GARCH component,  $\epsilon_{t-h}$  is the ARCH component, and  $\lambda$  captures asymmetric effects. If  $\lambda > 0$ , then the future conditional variance will increase more following a negative shock than following a positive shock of the same magnitude. Here,  $z_t$  is an independent and identically distributed random variable with zero mean and unit variance that follows a skewed- $t$  distribution, given by Fernández and Steel (1998):

$$f(z_{j,t}; \gamma) = \frac{2}{\gamma + \frac{1}{\gamma}} \left\{ f_v \left( \frac{z_{j,t}}{\gamma} \right) \mathbb{1}_{[0, \infty)}(z_{j,t}) + f_v(\gamma z_{j,t}) \mathbb{1}_{(-\infty, 0)}(z_{j,t}) \right\}$$

where  $\gamma$  is a skew parameter, and  $f_\nu$  is the density of the  $t$  distribution with  $\nu$  degree of freedom.

*Step 2. Finding the best fitting copula.*

Among the copulas, we find one with the best fit in Table 2 with empirical marginal distributions of  $R_t^\ell$ . We use an ML estimation method, that is,

$$\theta_i = \operatorname{argmax}_\theta \sum_{t=i}^{i+d} \ln c(\hat{u}_t, \hat{v}_t; \theta)$$

where  $c(\cdot, \cdot; \theta)$  is a copula density obtained by  $\partial^2 C(u, v; \theta) / \partial u \partial v$ ,  $\hat{u}_t$ , and  $\hat{v}_t$  are samples transformed from observations  $R_t^\ell$  by their empirical distributions obtained in step (1). To estimate  $\theta_i$ ,  $d$  days of samples  $(\hat{u}_t, \hat{v}_t)$  are used.

*Step 3. Computing  $\Delta \text{CoVaR}$ .*

We compute the time-varying  $\Delta \text{CoVaR}_t$  with the best fitting copula obtained in step (2) and marginal distributions in step (1), as stated in Proposition 4. To quantify the systemic impact of an asset price return on another asset price return, we compute the  $\beta$ -quantile  $\text{CoVaR}_{\beta,t}^{1|2}$  and  $\text{CoVaR}_{\beta,t}^{2|1}$  that are defined by

$$\mathbb{P}\left(R_t^1 \leq \text{CoVaR}_{\beta,t}^{1|2} | R_t^2 \leq \text{VaR}_{\alpha,t}^2\right) = \beta \text{ and } \mathbb{P}\left(R_t^2 \leq \text{CoVaR}_{\beta,t}^{2|1} | R_t^1 \leq \text{VaR}_{\alpha,t}^1\right) = \beta,$$

respectively. Then, we compute  $\text{CoVaR}_{\beta,t}^{1|2, \alpha=0.5}$  and  $\text{CoVaR}_{\beta,t}^{2|1, \alpha=0.5}$ .

To implement the first term of  $\Delta \text{CoVaR}$  in Proposition 4, the numerical inversion is needed for the Gaussian and Student  $t$  copulas. For the Gumbel and Clayton copulas with generator  $\psi$ ,  $C_\alpha^{-1}$  can be easily derived in an explicit form as  $\psi^{-1}(\psi(x) - \psi(\alpha))$  for  $x \in (0, \alpha)$ . Thus, (33) is written as

$$\text{CoVaR}_{\beta,t}^{1|2} = F_{R_t^1}^{-1}\left(\psi^{-1}(\psi(\alpha\beta) - \psi(\alpha))\right), \quad (22)$$

where  $\alpha$  and  $\beta$  are the given levels.

Next, for the second term of  $\Delta \text{CoVaR}$  in Proposition 4, computing the conditional copula function  $h_\alpha(u)$  with a given level  $\alpha$  is required as defined in (14). Depending on a choice of copulas, the functions  $h_\alpha(u)$  are obtained as analytic forms, which are derived by Aas et al. (2009) and Schepsmeier and Stöber (2014), as follows.

- Gaussian copula:

$$h_\alpha(u) = \Phi\left(\frac{\Phi^{-1}(u) - \theta\Phi^{-1}(\alpha)}{\sqrt{1 - \theta^2}}\right) \quad (23)$$

- Student  $t$  copula with the degree of freedom  $\nu$ :

$$h_\alpha(u) = t_{\nu+1} \left( \frac{t_\nu^{-1}(u) - \theta t_\nu^{-1}(\alpha)}{\sqrt{(\nu + [t_\nu^{-1}(\alpha)]^2)(1 - \theta^2)/(\nu + 1)}} \right) \quad (24)$$

- Gumbel copula: for  $x = (-\ln u)^\theta$  and  $y = (-\ln \alpha)^\theta$

$$h_\alpha(u) = -\frac{\exp\left(-(x+y)^{\frac{1}{\theta}}\right) \cdot (x+y)^{\frac{1}{\theta}-1} \cdot y}{\alpha \ln \alpha} \quad (25)$$

- Clayton copula

$$h_\alpha(u) = \alpha^{-\theta-1} \cdot \left(u^{-\theta} + \alpha^{-\theta} - 1\right)^{-1-\frac{1}{\theta}} \quad (26)$$

Dependence parameter  $\theta$  is the value estimated in step (2), and the level of  $\alpha$  is chosen as the median (i.e.,  $\alpha = 0.5$ ).

By conducting the three-step procedure described above, we compute the time-varying  $\Delta\text{CoVaR}$ 's. Then, we compare them with the calibrated parameters from the proposed model in Section 2 to examine the consistency of systemic risk measures for high frequency data.

## B. Proof of Proposition 4

As defined in (15), computing  $\Delta\text{CoVaR}$  consists of determining two types of CoVaR specified in (13) and (12). Each part is derived in the following step (i) and (ii).

(i) *The CoVaR defined in (12).*

It can be computed by using the property of a copula function. Then (12) can be written as

$$h_q \left( F_{R_t^j} \left( \text{CoVaR}_{\beta,t}^{d|j,\alpha=q} \right) \right) = \beta. \quad (27)$$

Thus, the CoVaR is given by

$$\text{CoVaR}_{\beta,t}^{i|j,\alpha=q} = F_{R_t^j}^{-1} \left( h_q^{-1}(\beta) \right). \quad (28)$$

(ii) *The CoVaR defined in (13).*

In this case, the quantile value of a conditional distribution, or, alternatively, of an unconditional bivariate distribution is needed if we express in (13) as

$$\frac{\mathbb{P} \left( R_t^i \leq \text{CoVaR}_{\beta,t}^{i|j}, R_t^j \leq \text{VaR}_{\alpha,t}^j \right)}{\mathbb{P} \left( R_t^j \leq \text{VaR}_{\alpha,t}^j \right)} = \beta. \quad (29)$$

Given that  $\mathbb{P}(R_t^j \leq \text{VaR}_{\alpha,t}^j) = \alpha$ , the CoVaR in (29) can be expressed as:

$$\mathbb{P}\left(R_t^i \leq \text{CoVaR}_{\beta,t}^{ij}, R_t^j \leq \text{VaR}_{\alpha,t}^j\right) = \alpha\beta. \quad (30)$$

Here, the form (29) can be expressed in terms of the joint distribution function of  $R_t^i$  and  $R_t^j$ ,  $F_{R_t^i, R_t^j}$ , as

$$F_{R_t^i, R_t^j}\left(\text{CoVaR}_{\beta,t}^{ij}, \text{VaR}_{\alpha,t}^j\right) = \alpha\beta, \quad (31)$$

and that, according to Sklar's theorem, the joint distribution function of two continuous variables can be expressed in terms of a copula function. Hence, (31) can be written as

$$C(u, v) = \alpha\beta, \quad (32)$$

where  $C(\cdot, \cdot)$  is a copula function,  $u = F_{R_t^i}(\text{CoVaR}_{\beta,t}^{ij})$  and  $v = F_{R_t^j}(\text{VaR}_{\alpha,t}^j)$ , and where  $F_{R_t^i}$  and  $F_{R_t^j}$  are the marginal distribution function of  $R_t^i$  and  $R_t^j$ , respectively. Given its copula representation in (32), the CoVaR can be computed from that equation through copulas in a two-step procedure. First, we obtain the value of  $u = F_{R_t^i}(\text{CoVaR}_{\beta,t}^{ij})$ . Since  $C(u, v) = \alpha\beta$ , where  $\alpha, \beta$ , and  $v$  are given (note that  $v = \alpha$ ), from the copula function specification we can solve to determine the value of  $u$ . Next, taking  $u$ , we can obtain the CoVaR value as the quantile of distribution  $R_t^i$ , with a cumulative probability equal to  $u$ , by inverting the marginal distribution function of  $R_t^i$ :  $\text{CoVaR}_{\beta,t}^{ij} = F_{R_t^i}^{-1}(u)$ . Letting  $C_\alpha^{-1}(\cdot)$  be the inverse of  $C_\alpha : x \rightarrow C(\cdot, \alpha)$ , then the CoVaR can be expressed as an analytic form

$$\text{CoVaR}_{\beta,t}^{ij} = F_{R_t^i}^{-1}\left(C_\alpha^{-1}(\alpha\beta)\right). \quad (33)$$

### C. More tests for calibration in Section 3

Some of selected estimates are presented in Table 3 with the numerically computed standard errors in the parentheses. In this period of time, the self-exciting term  $\alpha_{1s}$  of CL is close to zero and all other parameters are significant. Since we performed non-constraint parameter estimation, sometimes negative  $\alpha_s$  are observed, but it is better to be considered as zero by the Hawkes-based model definition. In general,  $\mu$  in CL is larger than that in RB implying larger trade frequency in CL and  $\beta$  in RB is larger than that in CL implying longer persistence in RB.

The estimates and numerically computed standard errors in parenthesis are presented in Table 4. Note that  $\alpha_{is}$  and  $\alpha_{ic}$  are similar to the estimates in Table 3 for  $i = 1, 2$ , which means that the additionally introduced  $\alpha_{in}$  and  $\alpha_{iw}$  do not affect the self- and mutually-exciting terms. The result also shows that  $\alpha_{in}$  are close to zero in the selected time period, which means that the price difference for narrowing events does not affect the intensities.

Table 3: Estimates for CL (left) and RB (right) under the Hawkes-based model without the flocking-related parameters

Date/Maturity	WTI crude oil				RBOB gasoline			
	$\mu_1$	$\alpha_{1s}$	$\alpha_{1c}$	$\beta_1$	$\mu_2$	$\alpha_{2s}$	$\alpha_{2c}$	$\beta_2$
2016-03-16	0.0780	0.0400	0.3710	0.5120	0.0577	0.3763	0.2001	0.9109
March 2016	(0.0025)	(0.0050)	(0.0122)	(0.0176)	(0.0017)	(0.0183)	(0.0110)	(0.0439)
2016-04-15	0.0731	0.0128	0.3455	0.4827	0.0593	0.5337	0.2126	1.3083
April 2016	(0.0025)	(0.0044)	(0.0119)	(0.0184)	(0.0014)	(0.0204)	(0.0118)	(0.0446)
2016-05-17	0.0872	-0.0206	0.3527	0.5106	0.0568	0.4200	0.2712	1.1314
May 2016	(0.0025)	(0.0037)	(0.0112)	(0.0195)	(0.0015)	(0.0204)	(0.0144)	(0.0510)
2016-06-16	0.1001	-0.0033	0.4315	0.6022	0.0574	0.3405	0.1954	0.8668
June 2016	(0.0027)	(0.0041)	(0.0124)	(0.0189)	(0.0016)	(0.0151)	(0.0101)	(0.0367)

We expand the time range, nonzero positive  $\alpha_{1n}$  of CL is also observed, but overall  $\alpha_{in}$  is quite small and close to zero. In addition,  $\alpha_{iw}$  are significant, which means that the price difference widening events increase the intensities so that the two price processes tend to converge to each other.

By data visualization, we confirm the previous discussion. For the graph, the selected maturity for the futures is February 2016 and estimates are computed on a daily basis over the sample period from January 4 to February 22, 2016. Figure 7 compares  $\alpha_n$  and  $\alpha_w$ . For both CL and RB, the estimated  $\alpha_n$  are almost zero, but  $\alpha_w$  are far from zero and  $\alpha_w$  in CL is larger than that in RB.

Figure 17 compares  $\alpha_s$  and  $\alpha_c$ . For CL,  $\alpha_s$  are close to zero and for other cases,  $\alpha_c$  in CL and  $\alpha_s$ ,  $\alpha_c$  in RB, the estimates are significantly positive. In addition,  $\alpha_s$  is less than  $\alpha_c$  in CL, but  $\alpha_s$  is greater than  $\alpha_c$  in RB over the sample period.

In Table 5, for each maturity, we calculated the averages of estimates on a daily basis using 20 days data. In this result, we also observe that  $\alpha_{in}$  are close to zero for all maturities.

#### D. Figures related to Section 4

Table 4: Estimates for CL (top) and RB (bottom) with the Hawkes flocking model

WTI crude oil						
date/maturity	$\mu_1$	$\alpha_{1n}$	$\alpha_{1w}$	$\alpha_{1s}$	$\alpha_{1c}$	$\beta_1$
2016-03-16	0.0755	-0.0120	0.2265	0.0105	0.4333	0.6079
March 2016	(0.0039)	(0.0086)	(0.0286)	(0.0053)	(0.0321)	(0.0523)
2016-04-15	0.0345	0.0046	0.1993	0.0076	0.2992	0.4084
April 2016	(0.0021)	(0.0078)	(0.0118)	(0.0038)	(0.0108)	(0.0160)
2016-05-17	0.0670	-0.0085	0.2053	-0.0318	0.3761	0.5699
May 2016	(0.0024)	(0.0069)	(0.0119)	(0.0032)	(0.0121)	(0.0217)
2016-06-16	0.0706	-0.0189	0.2748	-0.0121	0.4348	0.6142
June 2016	(0.0026)	(0.0093)	(0.0160)	(0.0032)	(0.0154)	(0.0245)
RBOB gasoline						
date/maturity	$\mu_2$	$\alpha_{2n}$	$\alpha_{2w}$	$\alpha_{2s}$	$\alpha_{2c}$	$\beta_2$
2016-03-16	0.0499	-0.0109	0.1335	0.4384	0.2306	1.2513
March, 2016	(0.0037)	(0.0083)	(0.0269)	(0.1005)	(0.0471)	(0.3109)
2016-04-15	0.0403	0.0098	0.1719	0.4450	0.1836	1.5166
April, 2016	(0.0013)	(0.0073)	(0.0112)	(0.0212)	(0.0125)	(0.0598)
2016-05-17	0.0413	0.0347	0.2229	0.4555	0.3085	1.4429
May, 2016	(0.0013)	(0.0096)	(0.0121)	(0.0200)	(0.0151)	(0.0492)
2016-06-16	0.0348	0.0186	0.1302	0.2950	0.1882	0.9146
June, 2016	(0.0014)	(0.0065)	(0.0077)	(0.0133)	(0.0096)	(0.0352)

Table 5: Means of estimates for CL and RB

maturity	WTI crude oil				RBOB gasoline			
	$\alpha_{1n}$	$\alpha_{1w}$	$\alpha_{1s}$	$\alpha_{1c}$	$\alpha_{2n}$	$\alpha_{2w}$	$\alpha_{2s}$	$\alpha_{2c}$
2016-01	-0.0229	0.1828	0.0003	0.3919	0.0197	0.1683	0.5835	0.2900
2016-02	-0.0332	0.2782	0.0106	0.4662	-0.0059	0.1290	0.4887	0.2605
2016-03	-0.0237	0.2481	-0.0129	0.4621	-0.0059	0.1321	0.4625	0.2491
2016-04	-0.0234	0.2161	-0.0266	0.4359	-0.0020	0.1517	0.4600	0.2333
2016-05	-0.0229	0.2497	-0.0233	0.4611	-0.0026	0.1480	0.4570	0.2577
2016-06	-0.0187	0.1725	-0.0250	0.4136	0.0174	0.1618	0.4737	0.2731
2016-07	-0.0157	0.2321	-0.0199	0.4300	0.0185	0.1872	0.4588	0.2579
2016-08	-0.0205	0.2013	-0.0149	0.4707	0.0026	0.1787	0.4498	0.2497
2016-09	-0.0145	0.2223	-0.0178	0.4870	-0.0015	0.1834	0.4574	0.2237
2016-10	-0.0115	0.2205	-0.0222	0.4970	0.0005	0.1738	0.4053	0.2212
2016-11	-0.0137	0.2123	-0.0164	0.4798	-0.0049	0.1576	0.4033	0.2123
2016-12	-0.0073	0.2756	-0.0242	0.4879	0.0028	0.1363	0.4169	0.2217

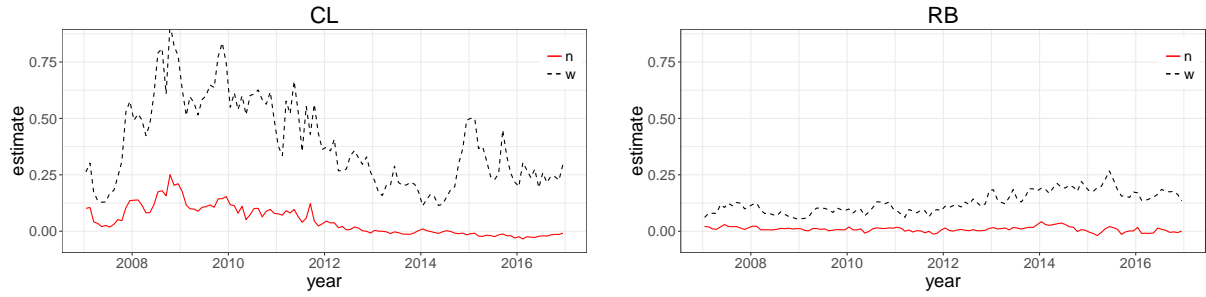


Figure 8: Comparison of changes in the flocking parameters  $\alpha_n$  (red line) and  $\alpha_w$  (black dotted line) for CL (left) and RB (right) from January 2007 to December 2016

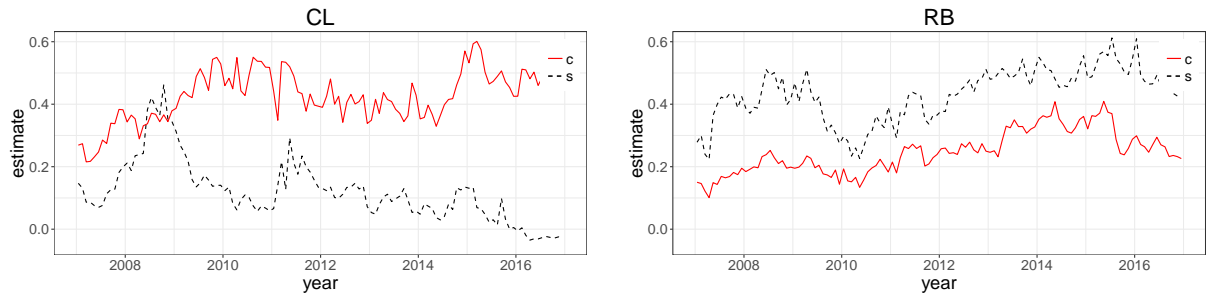


Figure 9: Comparison of changes in the self- and mutually exciting parameters  $\alpha_s$  (red line) and  $\alpha_c$  (black dotted line) for CL (left) and RB (right) from January 2007 to December 2016

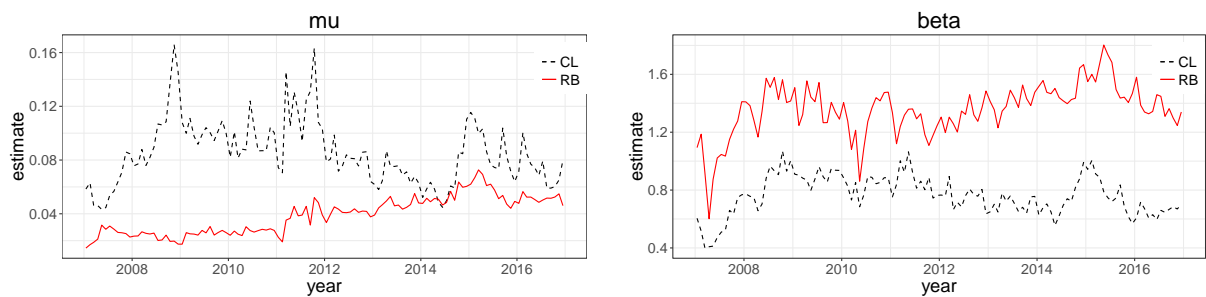


Figure 10: Comparison of changes in the exogenous fluctuation parameter  $\mu$  (left) and the persistence  $\beta$  (right) for CL (black dotted line) and RB (red line) from January 2007 to December 2016

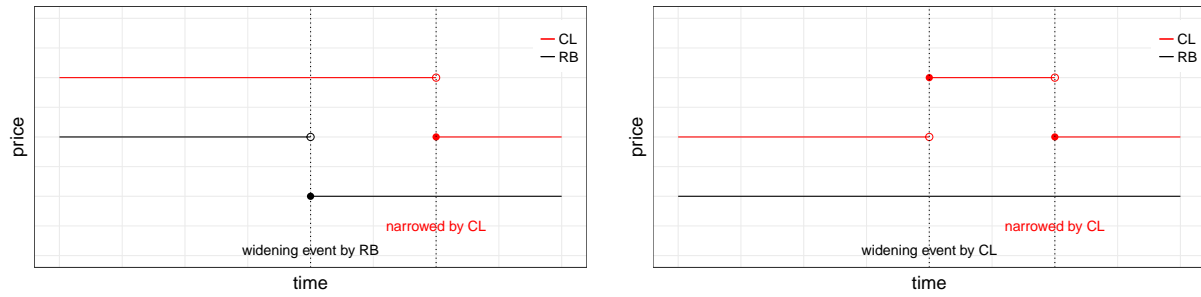


Figure 11: Examples of widening events and their possible consequences

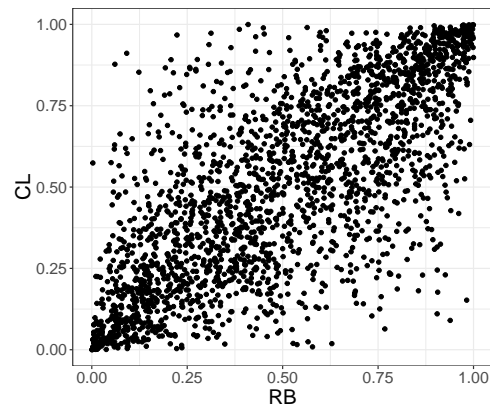


Figure 12: Scatter plot of  $\hat{u}_t, \hat{v}_t$  using the ARMA(1,1)-TGARCH(1,1) model with skewed- $t$  distribution

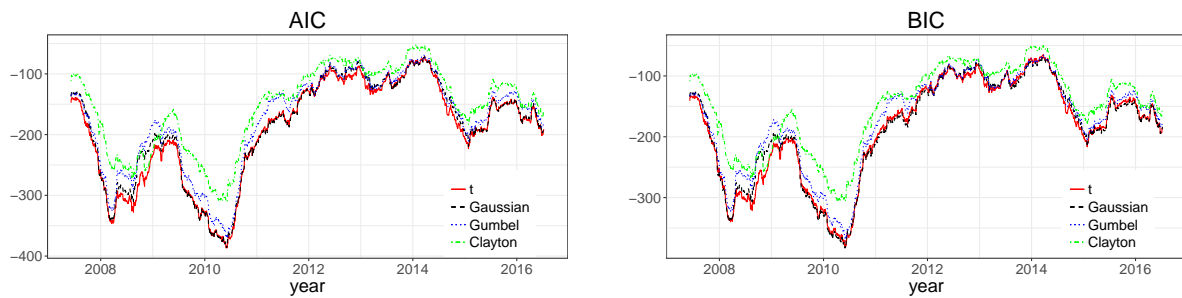


Figure 13: Results of AIC (left) and BIC (right) measures for Gaussian, Student  $t$ , Gumbel, and Clayton copulas from January 2007 to December 2016

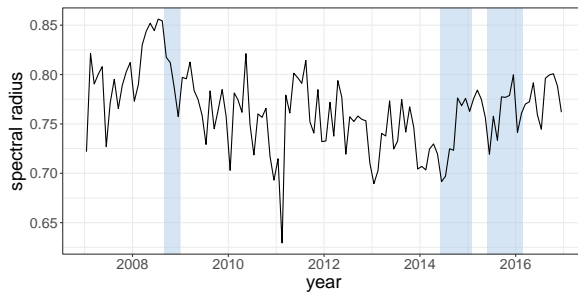


Figure 14: Illustration of spectral radius from January 2007 to December 2016

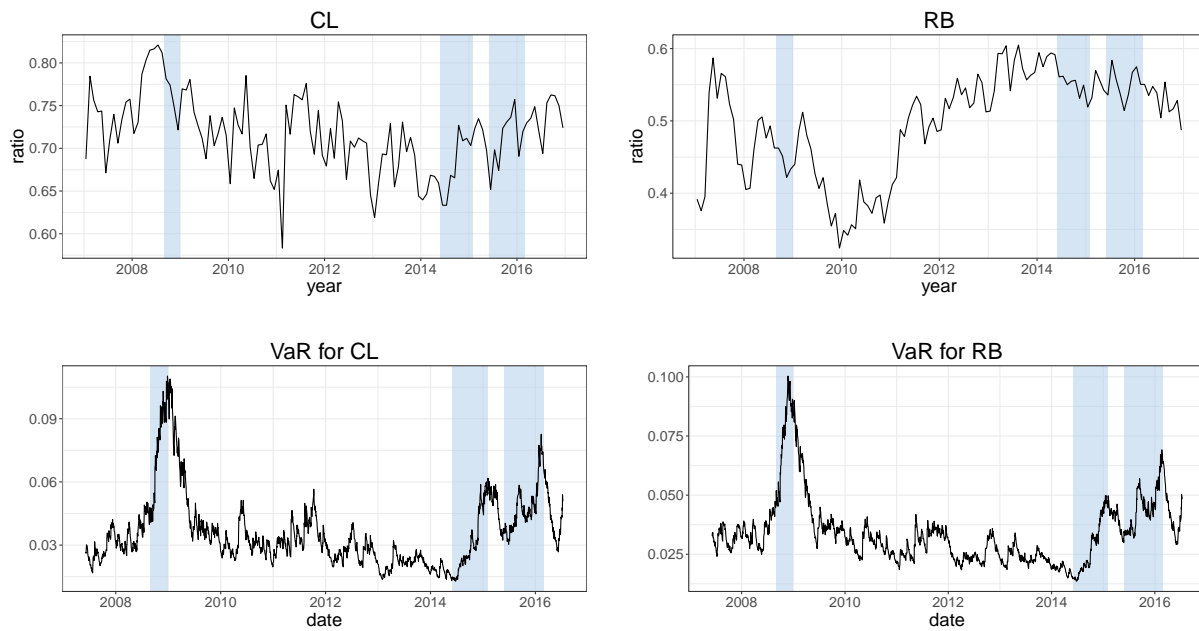


Figure 15: Illustration of evolution of  $(\alpha_{1s} + \alpha_{1c})/\beta_1$  for CL (top, left),  $(\alpha_{2s} + \alpha_{2c})/\beta_2$  for RB (top, right), time-varying one-day 95% VaR for CL (bottom, left), and VaR for RB (bottom, right) from January 2007 to December 2016

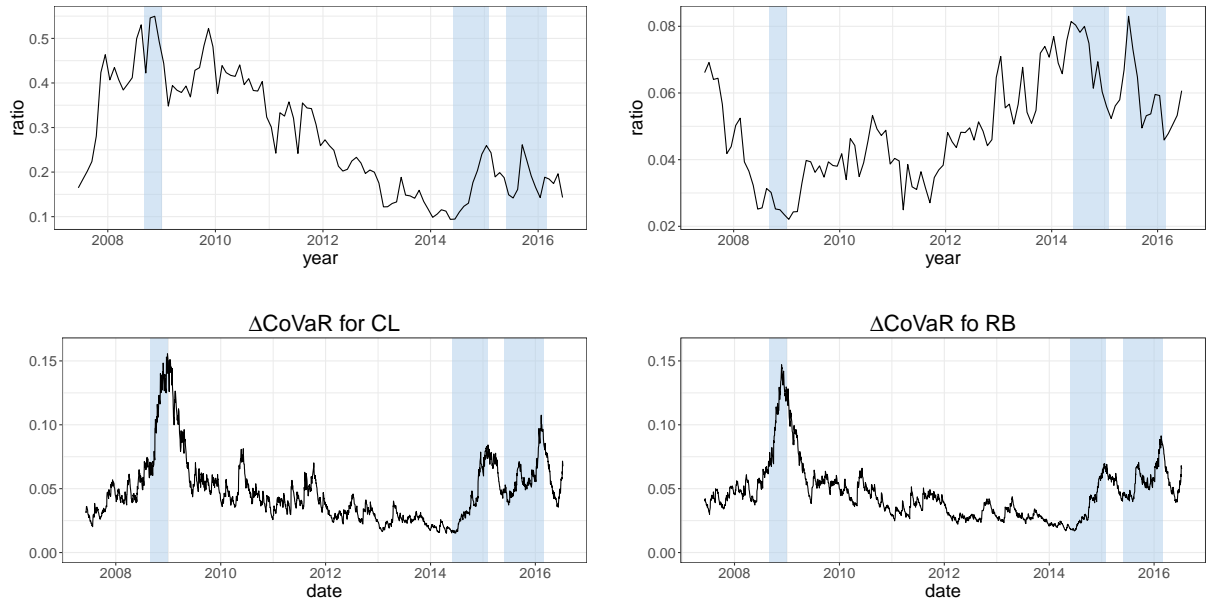


Figure 16: Illustration of evolution of  $(\alpha_{1n} + \alpha_{1w})/2\beta_1$  (top, left),  $(\alpha_{2n} + \alpha_{2w})/2\beta_2$  (top, right),  $\Delta\text{CoVaR}_t^{1|2}$  (bottom, left), and  $\Delta\text{CoVaR}_t^{2|1}$  (bottom, right) where  $R_t^1$  and  $R_t^2$  are given by the CL and RB daily returns at time  $t$ , respectively, from January 2007 to December 2016

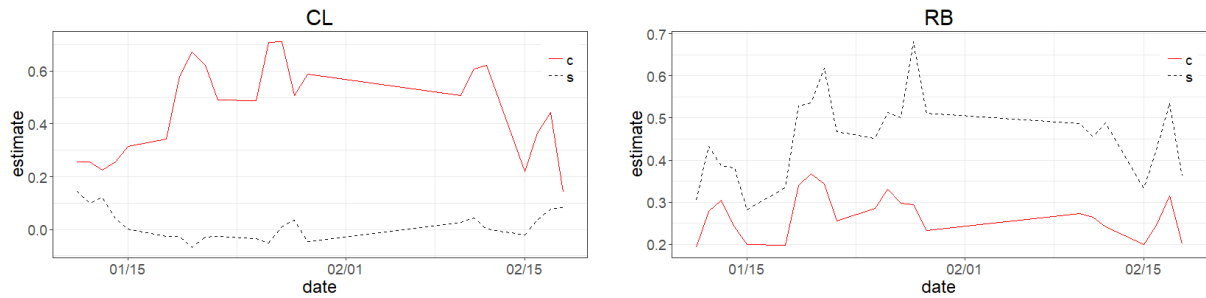


Figure 17: Comparison of  $\alpha_s$  and  $\alpha_c$  for CL (left) and RB (right) futures prices with maturity in February 2016

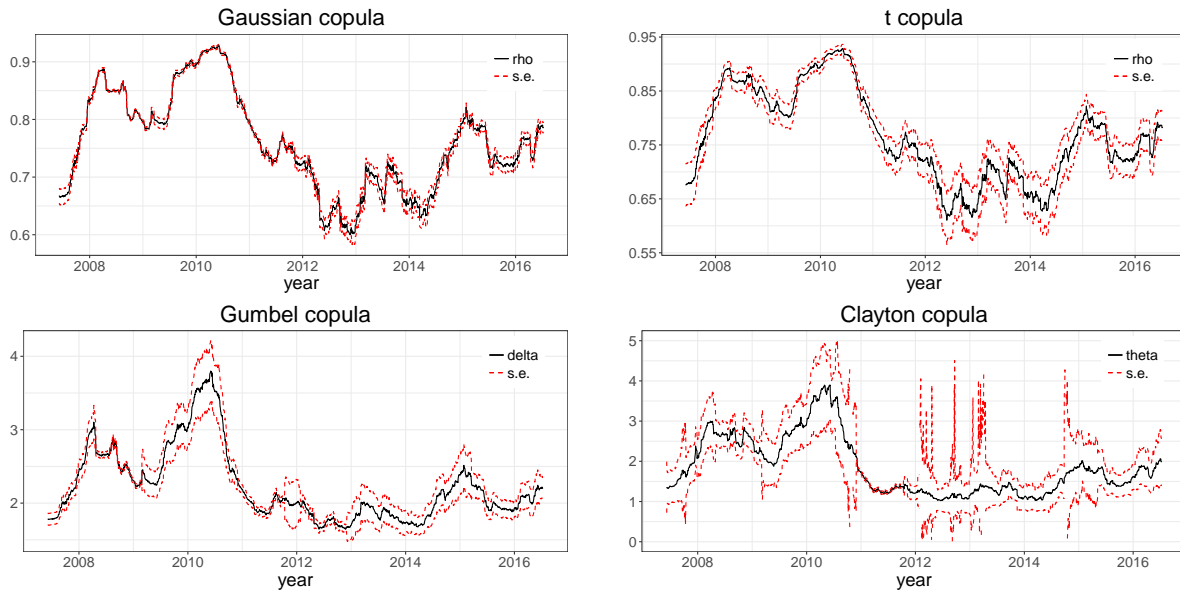


Figure 18: The evolution of the estimated dependence parameter  $\theta$  of CL and RB futures prices using Gaussian copula (top, right), Student  $t$  copula (top, left), Gumbel copula (bottom, left), and Clayton copula (bottom, right) with the standard error (red dotted line) from January 2007 to December 2016

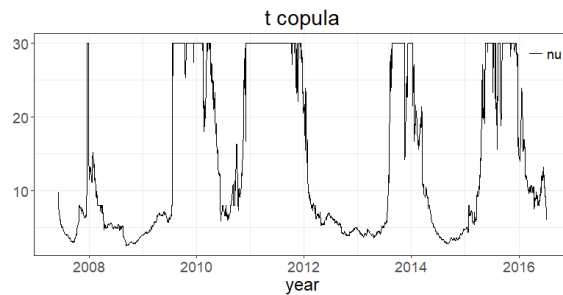


Figure 19: The evolution of the estimated degree of freedom parameter  $\nu$  in the Student  $t$  copula for the return pairs of CL and RB futures prices from January 2007 to December 2016

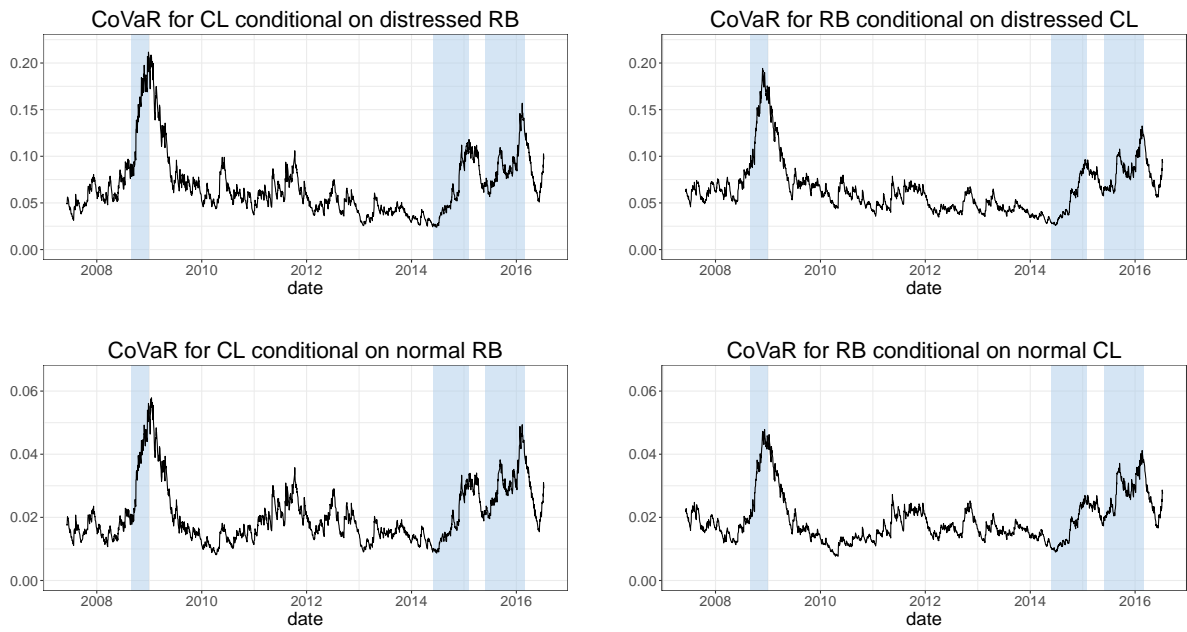


Figure 20: Illustration of time-varying one-day  $\text{CoVaR}_{95\%,t}^{1|2}$  (top, left),  $\Delta\text{CoVaR}_{95\%,t}^{2|1}$  (top, right),  $\text{CoVaR}_{95\%,t}^{1|2,\alpha=50\%}$  (bottom, left), and  $\Delta\text{CoVaR}_{95\%,t}^{2|1,\alpha=50\%}$  (bottom, right) where  $R_t^1$  and  $R_t^2$  are given by the CL and RB daily returns at time  $t$ , respectively, from January 2007 to December 2016